

ISTANBUL TECHNICAL UNIVERSITY ★ INSTITUTE OF ENERGY

**HYDROGEN ADSORPTION ON FUNCTIONALIZED SINGLE-WALLED
CARBON NANOTUBES: A DFT STUDY**

M.Sc. THESIS

Süha Erhan Ünal

Energy Science and Technology Department

Energy Science and Technology Programme

September 2012

ISTANBUL TECHNICAL UNIVERSITY ★ INSTITUTE OF ENERGY

**HYDROGEN ADSORPTION ON FUNCTIONALIZED SINGLE-WALLED
CARBON NANOTUBES: A DFT STUDY**

M.Sc. THESIS

Süha Erhan Ünal

(301091075)

Energy Science and Technology Department

Energy Science and Technology Programme

Thesis Advisors: Prof. Nilgün Karatepe-Yavuz

Assist. Prof. Adem Tekin

September 2012

İSTANBUL TEKNİK ÜNİVERSİTESİ ★ ENERJİ ENSTİTÜSÜ

**FONKSİYONLAŞTIRILMIŞ TEK DUVARLI KARBON NANOTÜPLERDE
HİDROJEN ADSORPSİYONU: DFT ÇALIŞMASI**

**Yüksek Lisans Tezi
Süha Erhan ÜNAL
(301091075)**

**Enerji Bilimi ve Teknoloji Anabilim Dalı
Enerji Bilimi ve Teknoloji Programı**

**Tez Danışmanları : Prof. Dr. Nilgün Karatepe-Yavuz
Yrd. Doç. Dr. Adem Tekin**

Eylül 2012

Süha Erhan Ünal, a M.Sc. student of ITU Institute of Energy student ID 301091075, successfully defended the thesis entitled “HYDROGEN ADSORPTION ON FUNCTIONALIZED SINGLE-WALLED CARBON NANOTUBES: A DFT STUDY”, which he prepared after fulfilling the requirements specified in the associated legislations, before the jury whose signatures are below.

Thesis Advisor : **Prof. Nilgün KARATEPE-YAVUZ**

Istanbul Technical University

Co-advisor : **Assist. Prof. Adem TEKİN**

Istanbul Technical University

Jury Members : **Prof. Mine YURTSEVER**

Istanbul Technical University

Assoc. Prof. F. Aylin KONUKLAR

Istanbul Technical University

Assist. Prof. Fatih ÖZTÜRK

Istanbul Technical University

Date of submission: **10 June 2012**

Date of defence examination: **11 September 2012**

*To my dear friend, Burak Ümit GEDİK,
lost in a terrible accident during his military service*

FOREWORD

I would like to express my sincere gratitude to my co-supervisors Prof. Nilgün KARATEPE-YAVUZ and Assist. Prof. Adem TEKİN for her/his concern, advices and encouragement during this study.

My special thanks to my parents and little brother, for their understanding and complete support to me with all my decisions. Last but not the least I would like to thank my dear Seçil KELEŞ for her understanding and pure love.

September 2012

Süha Erhan ÜNAL
(Chemical Engineer)

TABLE OF CONTENTS

	<u>Page</u>
FOREWORD	xi
TABLE OF CONTENTS	xiii
ABBREVIATIONS	xv
LIST OF TABLES	xvii
LIST OF FIGURES	xix
SUMMARY	xxi
ÖZET	xxiii
1.INTRODUCTION	1
2.STORAGE OF HYDROGEN	3
2.1.Gas and Liquid Storage.....	3
2.2.Solid Storage.....	4
2.2.1.Metal hydrides.....	4
2.2.2.Metal organic framework.....	4
2.2.3.Carbon materials.....	5
2.2.3.1.Activated carbons (ACs).....	5
2.2.3.2.Graphite nanofibers (GNFs).....	6
2.2.3.3.Single Walled Carbon Nanotubes (SWNTs).....	6
3.SINGLE-WALLED CARBON NANOTUBES	7
3.1.Structure of Single-Walled Carbon Nanotube.....	7
3.2.Properties of Carbon Nanotubes.....	8
3.2.1.Chemical properties of carbon nanotubes.....	8
3.2.2.Electrical properties of carbon nanotubes.....	8
3.2.3.Solubility of carbon nanotubes.....	9
3.3.Purification of carbon nanotubes.....	10
3.3.1.Chemical oxidation.....	10
3.3.2.Physical Purification.....	11
3.3.3.Multi-step purification.....	12
3.4.Functionalization of carbon nanotubes.....	12
3.4.1.Non-covalent functionalization.....	12
3.4.2.Covalent functionalization.....	14
3.5.Hydrogen adsorption on functionalized carbon nanotubes.....	16
4.COMPUTATIONAL METHODS	21
4.1.Density Functional Theory.....	21
4.1.1.Hohenberg and Kohn's theorem.....	22
4.1.2.Kohn Sham's theorem.....	23
4.1.3.Reciprocal space and k points.....	24
4.1.4.The Energy cut-off and pseudopotentials.....	25

5.RESULTS AND DISCUSSION.....	27
5.1.Computational Setup	27
5.2.Defect Generation and Hydrogen Adsorption	27
5.2.1.Defect generation and oxidative functionalization	27
5.2.2.The hydrogen adsorption on oxidized SWNT	31
5.3.Hydrogen adsorption on metal doped, oxidized SWNTs	34
5.3.1.Ni and Ti doped oxidized SWNT's	35
5.3.2.Hydrogen adsorption on Ni and Ti doped, oxidized SWNTs.....	36
5.3.3.Metal doped oxidized SWNT's	39
5.3.4.Hydrogen adsorption on metal doped oxidized SWNT's.....	40
5.3.5.Clustering of metals	45
6.SUMMARY, CONCLUSIONS AND FUTURE WORK.....	51
REFERENCES.....	53
CURRICULUM VITAE	59

ABBREVIATIONS

CNT	: Carbon Nanotube
MOF	: Metal Organic Frame-Work
AC	: Active Carbon
CNF	: Carbon Nanofiber
CVD	: Chemical Vapour Deposition
CCVD	: Catalytic Chemical Vapour Deposition
SWNT	: Single Wall Carbon Nanotube
MWCNT	: Multi Wall Carbon Nanotube
DFT	: Density Functional Theory
RPBE	: Revised Perdew–Burke–Ernzerhof
Atm	: Atmosphere pressure
TGA	: Thermal Gravimetric Analysis
nm	: Nano meter
µm	: Micro meter
pm	: Picometer
°C	: Degree Celsius
eV	: Electron-Volt

LIST OF TABLES

	<u>Page</u>
Table 5.1 : Binding energies of hydrogen molecules on (111), (115), (131) and (135) sites of the oxidized SWNT.....	33
Table 5.2 : Adsorption energies of Ni and Ti metals on 13 different adsorption site of the oxidized SWNT.....	36
Table 5.3 : Adsorption energies of hydrogen on Ni and Ti doped (111), (115), (115) and (135) sites of oxidized SWNT.....	37
Table 5.4 : Binding site of single adatom on (111) and (131) of (8,0) oxidized SWNT.....	39
Table 5.5 : Binding energies [in eV] of the oxidized SWNT's doped by four metal atoms at -OOH, R-OH and circumferential sites.....	46

LIST OF FIGURES

	<u>Page</u>
Figure 3.1 : Scheme of sp^2 hybridization in graphene; σ bonds, π bonds and their... 8 energies with respect to Fermi level	8
Figure 3.2 : Schematic representation of the oxidatively induced cutting and..... 9 generation of carboxylic acid functionalities.....	9
Figure 3.3 : Derivatization strategies for carbon nanotubes: (a) noncovalent 13 exohedral functionalization with functional moieties based on specific CNT–molecule interactions (b) endohedral functionalization (C_{60} incorporation) (c) defect-group functionalization (d) direct covalent sidewall functionalization	13
Figure 3.4 : Representation of the oxygen-containing surface groups on CNTs..... 14	14
Figure 3.5 : Reactant (1), products (5 and 5'), transition state (TS1) and 16 intermediates (2, 3, and 4) found on the proposed functionalization pathway of the model. The inset shows the -COOH functional group grafted on the di-vacancy formed on the graphene sheet at the end of the reaction.....	16
Figure 3.6 : Defected (a) (8,2) and (b) (6,4) nanotubes. Light colored portion..... 17 indicates the presence of octagon and pentagons in the nanotube.....	17
Figure 5.1 : a) Plane (8,0) zigzag SWNT b) DOS. Fermi level is indicated with red dashed line.	27
Figure 5.2 : a) SWNT having single vacancy on sidewall. b) DOS of the whole system. c) PDOS of carbon atom shown as yellow. Two dangling carbon atoms are indicated with orange. Fermi level is indicated with the red dashed line.	29
Figure 5.3 : a) The relaxed vacancy defect oxidized (8,0) SWNT. b) DOS of thewhole system. c) PDOS of carbon atom indicated with yellow. d) PDOS of COOH group. Representing colors: carbon: grey; oxygen: red; hydrogen: white. Two dangling carbon atoms are indicated with orange. Fermi level is indicated with red dashed line... 30	30
Figure 5.4 : Adsorption sites on the oxidized SWNT..... 32	32
Figure 5.5 : Adsorption of hydrogen on (111), (115), (131) and (135) sites of theoxidized SWNT	33
Figure 5.6 : Selected metals	35
Figure 5.7 : Hydrogen adsorption on Ni, Ti doped (111), (115), (131) and (135) sites.....	38
Figure 5.8 : Hydrogen binding energies [eV] onto the metal doped oxidized SWNT's	42

Figure 5.9 : Hydrogen adsorbed geometries of (111) metal doped oxidized SWNT's.	43
Figure 5.10: Hydrogen adsorbed geometries of (131) metal doped oxidized SWNT's.	44
Figure 5.11 : Optimized geometries of Ca, Fe and Ni clustered oxidized SWNT...	48
Figure 5.12 : Optimized geometries of Pd, Pt and Ti clustered oxidized SWNT.....	49

HYDROGEN ADSORPTION ON FUNCTIONALIZED SINGLE WALL CARBON NANOTUBES: A DFT STUDY

SUMMARY

The discovery of carbon nanotubes (CNTs) in 1991 attracted a great deal of attention. CNTs are today one of the key elements of nanotechnology and are most intensively investigated materials. CNTs with their high mechanical, electrical, thermal and chemical properties are regarded as promising materials for many different potential applications such as electronic devices, electrodes, drug delivery systems, hydrogen storage and so forth.

Although hydrogen is one of the most abundant element in nature, it can't be directly used as a fuel source, generally preferred as a back-up source due to non-effective storage conditions. The discovery of high hydrogen storage capacity of carbon nanotubes makes up alternatives for hydrogen storage systems. The enhancement of hydrogen adsorption capacity via metal doping and defect functionalization has begun to find a place incrementally in researcher's mind. However, no one has tried to examine the adsorption capacity in a complete fashion (a screening including most of the transition metals) using computational models under both of these circumstances up-to-date.

In this study, hydrogen adsorption on side-wall oxidized (8,0) single wall nanotubes (SWNT) decorated with metals was investigated using a periodic density functional theory (DFT) employing RPBE exchange-correlation functional. First, on the surface of SWNT, a single vacancy has been formed and subsequently this vacant site has been oxidized with a carboxylic acid group (-COOH). It has been found that hydrogen does not bind to the oxidized SWNT. Therefore, the SWNT was decorated with metal atoms to reach a reasonable hydrogen binding. Since there are many possible positions to dope the metal atoms on the oxidized SWNT, the most important ones were determined with the help of computations involving Ni and Ti. Then, the other metal species considered in this study (Ca, Co, Cr, Fe, Mn, Pd, Pt, Rh, Ru, Sc, V, Y) were also doped on these most promising positions. Following the metal decoration, a single hydrogen molecule was adsorbed on SWNT. Hydrogen adsorption was found acceptable SWNT's doped with Ni, Pd and Pt. Finally, the question "which metals tend to clustering" was tried to be answered. For this purpose, Ni, Ti, Pd, Pt, Fe and Ca were clustered on the oxidized SWNT. It has been observed that all metals do clustering and this fact significantly reduces the amount of adsorbed hydrogen on the SWNT.

FONKSİYONLAŞTIRILMIŞ TEK DUVARLI KARBON NANOTÜPLERDE HİDROJEN ADSORPSİYONU: DFT ÇALIŞMASI

ÖZET

Hidrojen doğada en çok bulunan elementlerden biri olmasına rağmen, depolama şartları yaygın kullanım için elverişli olmadığı için direkt olarak enerji kaynağı olarak kullanılamamakta, genel olarak yedek kaynak olarak tercih edilmektedir. Karbon nanotüplerin yüksek hidrojen adsorplama özelliği, hidrojen depolama sistemleri için onları önemli alternatif yapmaktadır. 1991 yılında keşfedilmeleri ile büyük ilgi uyandıran karbon nanotüpler, günümüzde nano teknolojinin vazgeçilmez unsurlarından biridir ve yoğun olarak araştırılan malzemelerdendir. Mekanik, kimyasal, ısıl ve elektriksel özelliklerinin çok iyi olması sebebiyle; elektronik malzemeler, elektrotlar, ilaç taşıma sistemleri, hidrojen depolama gibi birçok farklı potansiyel uygulama için umut vaat etmektedirler. Dillion ve arkadaşları saflaştırılmamış nanotüplerde hidrojen adsorplama kapasitesi üzerine çalışmalarıyla, hidrojen depolama alanında karbon nanotüpleri ele alan ilk çalışmayı gerçekleştirmişlerdir. Department of Energy (DOE)'nin 2015 yılı hedefi olan kütlece % 9 hidrojen depolama kapasitesine ulaşmak amacıyla, metal ilavesi veya yapısal bozuklukların fonksiyonlaştırılması yoluyla hidrojen adsorpsiyon kapasitesinin artırılması, araştırmacıların üzerinde yoğunlaşmaya başladığı konulardan biridir. Ancak, bu iki koşul altında hidrojen adsorpsiyon kapasitesini, yoğunluk fonksiyonel teorisi (YFT) kullanarak günümüze kadar kimse araştırmamıştır.

Bu çalışmada, periyodik YFT kullanılarak, yan duvarı oksitlenmiş ve geçiş metali ilave edilmiş/edilmemiş (8,0) zigzag tek duvarlı karbon nanotüplerin hidrojen adsorpsiyon kapasitesi incelenmiştir. Amaç, hidrojenlerin nanotüp yapısı ile en uygun koşullarda bağ kuracak şekilde, uygun yapının tayin edilmesidir. Hidrojen, karbon yapılar üzerinde iki şekilde tutunmaktadır: moleküler formda fiziksel adsorpsiyon yaparak veya atomik formda kimyasal adsorpsiyon yaparak. Kimyasal adsorpsiyonda, hidrojen ve depolama malzemesi arasında kurulacak olan kimyasal bağ ne kadar kuvvetli olursa, depolanmış olan hidrojenin salınması için o kadar büyük enerji harcanacaktır. Hidrojen ve depolama malzemesi arasında kurulacak bağlanma enerjisi 0.2-0.6 eV aralığında iken, en uygun adsorpsiyon koşullarının sağlandığı literatürde kabul edilmiş bir gerçektir. Hesaplamalar sonucu elde edilen tüm bağlanma enerjileri, bu referans aralığı ele alınarak değerlendirilmiştir.

Periyodik YFT hesaplamaları, DACAPO kodu içerisinde, RPBE değişken korelasyon fonksiyoneli kullanılarak yürütülmüştür. Hesaplamalarda kullanılan (8,0) tek duvarlı karbon nanotüp, $21.3 \text{ \AA} \times 16.3 \text{ \AA} \times 8.54 \text{ \AA}$ boyutlarına sahip ortorombik birim hücresi içerisinde tanımlanmıştır. Periyodik hesaplamalarda kullanılan, birim hücre içerisindeki her bir yapı, aralarındaki etkileşimimi yok etmek amacıyla, birbirinden 10 \AA uzaklıklara yerleştirilmiştir. Çalışmada, öncelikle (8,0) tek duvarlı

nanotüpün temel yapısı ve atomik boşluk içeren bölge tayin edildikten sonra, boşluk oluşumuna bağlı olarak elektriksel özelliklerindeki değişimler incelenmiştir. (8,0) tek duvarlı nanotüp, pürüzsüz halde yarı-iletken formda iken, boşluk oluşumu ile birlikte iletken özellik kazanmıştır. Kimyasal oksidasyon sonucu oluşabilecek oksit gruplarının temelini, nanotüp duvarı üzerindeki, hegzagonal yapısı bozulmuş karbon atomları olduğu önceki literatür çalışmalarından bilinmektedir. Yan duvar üzerinde oluşturduğumuz oksidatif fonksiyonel yapı, nanotüp duvarına ve nanotüp çemberinin normal eksenine dik pozisyonda lokal minimuma sahiptir ve bu literatür çalışmaları ile örtüşmektedir. Hidrojen molekülleri karboksilik grup çevresindeki ve grubun silindir merkezine göre ters tarafındaki (karboksilik grubun etkisinden bağımsız bölge) hegzagonal boşluklara ayrı ayrı çalışmalarda yerleştirilmiş ve bağlanma enerjileri hesaplanmıştır. Ne yazık ki, hidrojenin karboksilik grup çevresinde bağlanmadığı görülmüştür. Literatürde, nanotüp duvarı üzerinde metal yerleştirilmesi yoluyla, hidrojen adsorpsiyon kapasitesinin artırıldığı, deneysel ve teorik çalışmalarla gösterilmiştir. Bundan dolayı, ikinci aşamada, okside olmuş yapı üzerine 13 değişik hegzagonal pozisyonlarda, on dört farklı metalin (Ca, Co, Cr, Fe, Ni, Mn, Pd, Pt, Rh, Ru, Sc, Ti, V ve Y) ilavesi gerçekleştirilmiştir.

Metal ilavesi çalışmaları için öncelikle, seçilen iki metal (Ni ve Ti) hegzagonal boşluklara ayrı ayrı yerleştirilmiş ve metalin tutunması için en uygun bölgeler, karboksilik asit çevresinde oluşan boşluklar olarak tayin edilmiştir. Daha sonra, iki metal için karboksilik asit çevresindeki iki bölge ve karboksilik asitten en uzak iki bölge olmak üzere, dört hegzagonal bölge üzerinde hidrojen adsorpsiyon bağlanma enerjileri hesaplanmış ve literatür çalışmaları ile karşılaştırılmıştır. Okside olmuş nanotüp ile çok kuvvetli bağ yapan Ti metalinin, hidrojen adsorpsiyon kapasitesinin düşük olduğu belirlenmiştir. Sonraki aşamada, diğer on iki metalin (Ca, Co, Cr, Fe, Mn, Pd, Pt, Rh, Ru, Sc, V ve Y) de en uygun iki yapı üzerinde (karboksilik asitin önü ve arkası) tutunması sağlandıktan sonra, hidrojen adsorpsiyon bağ enerjileri incelenmiştir. Okside olmuş tek duvarlı nanotüp ile nispeten zayıf bağ yapan Ni, Pd ve Pt gibi metallerin istenilen 0.2-0.6 eV bağ enerjisi aralığında hidrojen depolayabildiği tespit edilmiştir.

Metallerin kümelenmeye olan yatkınlıkları literatür çalışmalarından bilinmektedir. Bazı literatür çalışmalarında, oksidatif fonksiyonlaştırılmamış yapılarda metal kümelenmesi yoluyla hidrojen depolama kapasitesinin düştüğü belirtilmektedir. Bu nedenle, okside olmuş nanotüpler üzerinde 6 metal için (Ca, Fe, Ni, Pd, Pt ve Ti) küme oluşup oluşmadığı üç farklı yapı (karboksilik grup çevresinde, karboksilik gruptan en uzak pürüzsüz nanotüp yüzeyi üzerinde ve nanotüp çevresinde tek tek yerleştirilmiş halde) kullanılarak incelenmiştir. Paladyum hariç tüm metallerin karboksilik grup üzerinde/çevresinde kümelenmeyi tercih ettiği bulunmuştur. Paladyum ise, nanotüpün pürüzsüz olan yüzeyinde kümelenmeyi tercih etmektedir. Fakat bu durum artan metal atomu sayısıyla değişebilir. Ancak, hiçbir metal kümelenme oluşturmadan nanotüp çevresinde tek tek tutunmayı tercih etmemektedir. Metaller kümelenme yaptıkları için bağlanan hidrojen miktarlarında düşme gerçekleşecektir.

Gerçekleştirilen bu çalışma ile literatürde hiç değinilmemiş bir konu olan oksidatif fonksiyonlaştırılmış tek duvarlı karbon nanotüp üzerinde, metal ilaveli/ilavesiz durumlarda hidrojen adsorpsiyon bağlanma enerjileri belirlenmiş ve

karşılaştırılmıştır. Daha sonraki çalışmalar için, daha büyük bir birim hücre kullanılarak, metal kümelenmesi oluşturmuş oksidatif yapılar üzerinde karboksilik grubun olumsuz etkisini bertaraf edecek optimum metal atomunun saptanabileceği ve hidrojen adsorpsiyon kapasitelerinin incelenebileceği önerilmiştir.

1. INTRODUCTION

The continuous increases in the level of hazardous emissions and the issue of more stringent environmental regulations have led to the development of more efficient and less hazardous methods of power generation. Significant research and development activities are being carried out to increase the efficiency of hydrogen storage systems to make them competitive with current fossil fuels for transportation and stationary applications, and with batteries for portable applications. The overwhelming advantage of hydrogen as an energy source lies in the fact that it is one of the most abundant found in nature as well as can be easily regenerated, therefore constituting a true renewable energy carrier. It is always desirable to develop a new storage material with high capacity, light mass and high stability, which may be applicable for portable electronics and moving vehicles. Carbon nanotubes seem to be an ultimate alternative for this, since nanotubes are chemically stable and have low mass density. In order to develop and demonstrate viable hydrogen storage technologies, a set of objectives have been asserted by the US Department of Energy (DOE), based on achieving a driving distance of 500 km for a hydrogen powered vehicle. These objectives [1] fix a target of of 3 kWh/kg (9 wt.%), 2.7 kWh/l and \$2 kWh for 2015. It is important to note that these are system targets, which implies that the weight of the storage system as a whole must be taken into account.

A promising storage alternative for hydrogen systems relies on the chemical or physical binding of hydrogen with other elements. This can be achieved through sorption of hydrogen on or in a solid substrate, relying either on physisorption or chemisorption processes (or a combination of both), or through the chemical storage of hydrogen in organic liquids or others.

Storage by sorption processes on the surface of materials has been widely studied for hydrogen storage applications in the last few years [1, 2]. Carbon-based nanoporous materials such as activated carbons (AC), single-walled carbon nanotubes (SWNTs)

and metal–organic frameworks (MOFs) have been proposed as promising adsorbents for hydrogen [1, 2]. The interest in these materials lies in the fact that they can be optimized for hydrogen storage through various physical and chemical treatments.

In this manner, first of all carbon nanotubes were under debate because CNTs are the blue boy of the recent scientific activities and there are also so many subjects that could be searched. As a lot of researchers were aware of this opportunity, storage capacity of carbon nanotubes [3-11] or modified carbon nanotubes (for example metal doped CNTs) [12-16] or also oxidative functionalized carbon nanotubes [17] are being carried out in last two decades. But, a point still remains unclear and waits to be developed by researchers: what the adsorption potential of both metal doped and oxidative-functionalized CNTs is.

Since it has already been proven [18] that CNTs might have several defects, oxidized groups or vacancies existed on the tube wall and open ends due to the purification. The purification is an essential for removing carbonaceous impurities and metal catalyst, but harmful since deforming tube wall and producing defects, vacancies and also oxide- groups. In this study, the adsorption potential of SWNT with oxidative-functionalized and metal doped is tried to calculate by Density Functional Theory (DFT).

Chapter 2 contains storage types of hydrogen alongside of that Chapter 3 contains detailed info about SWNT's. Short brief has been given about DFT in computational methods, Chapter 4. Finally, major results obtained from experimental studies and computational calculations are presented in results and discussion, Chapter 5. And finally, summary, conclusions and recommendations for further studies are committed in Chapter 6.

2. STORAGE OF HYDROGEN

Investigations of alternative energy strategies have recently become important, particularly for future world stability. Considering that mature renewable energy sources, such as wind and solar, are not so reliable, not ever ready sources. There is generally a variation on power load while producing energy.

Hydrogen is not actually a major energy sources, generally called energy carrier. Under these circumstances, backing up produced excessive energy by introducing into hydrogen and storing is to be a stroke of genius. Beside this, directly using hydrogen as a major energy source instead of conventional fuels is under debate way for future generation. According to recent studies, fuel cells are the most appropriate tool to produce energy from hydrogen [19-21].

2.1. Gas and Liquid Storage

The most traditional way of storing hydrogen is in the gaseous form in pressure vessels. For compressed storage of hydrogen, the gas is usually compressed to pressures between 200 and 350 bar though, more recently, storage pressures of 700 bars in cylindrical stainless steel and aluminium alloys tank [22]. The drawback of this process is that hydrogen has a tendency to adsorb and dissociate to the atomic hydrogens at material surfaces, then diffuses into the material which causes embrittlement of the storage material and leakage of gas.

Liquid hydrogen is light and has less potential risks in terms of storage pressure compared with the compressed gas. However, the hydrogen liquefies at $-253\text{ }^{\circ}\text{C}$ and thus sophisticated insulation techniques are required for the storage vessels. Another problem is energy need to liquefy the hydrogen that requires about 30% of the energy content of hydrogen [22].

2.2. Solid Storage

Hydrogen is an extremely volatile gas under ambient conditions, resulting in a low volumetric energy density for practical applications. For on-board use, hydrogen must be compressed to very high pressures or stored cryogenically, both of which cost energy and substantially increase vehicle weight. The goal therefore is to design low-cost, light-weight materials that can reversibly and rapidly store hydrogen near ambient conditions at a density equal to or greater than liquid hydrogen. In this respect, several investigations such as metal hydrides, MOFs and carbon materials were discussed in detail below.

2.2.1. Metal hydrides

Certain metals and alloys can repeatedly absorb and release hydrogen under moderate pressures and temperatures via the formation of hydrides. Heat must be removed during absorption of the hydrogen, but has to be added to effect desorption. The metal hydrides can be categorized as high, medium- or low temperature systems [23].

Among the gravimetric density enhancement researches, most intriguing chemical composite material is sodium borohydride. It releases hydrogen via an irreversible reaction with water, which means 50% of the produced hydrogen coming from the water. According to Wu's study, 30 wt % solution of sodium borohydride is the second-best hydrogen carrier after liquid hydrogen [24].

2.2.2. Metal organic framework

Metal-organic frameworks (MOFs) are crystalline solids that are assembled by the connection of metal ions or clusters through molecular bridges. Metal-organic frameworks can display outstanding performance characteristics with high surface areas, up to 1000 m²/g [25] for cryogenic hydrogen storage at 77 K and pressures up to 100 bar [26]. In particular, a rapid and fully reversible H₂ uptake of 10.0 total wt.% and 66 g L⁻¹ has been observed for Zn₄O(BDC)₃ [26].

2.2.3. Carbon materials

Carbon nano-materials are very attractive candidates for hydrogen storage because of owning of high specific surface area, micro porosity, low mass and good adsorption ability [21].

Hydrogen adsorption mechanism comprises two ways: physisorption and chemisorption. Physisorption is based on the Van der Waals interaction between gases and solids. Since weak hydrogen interaction occurs between the substrate surface and hydrogen molecule, hydrogen is desorbed with increasing temperature [1].

Physisorption is a completely reversible process that hydrogen can be easily adsorbed and desorbed during several cycles without any losses. At a given temperature, the amount of gas adsorbed is only a function of the pressure and is desorbed when pressure decreases. Since no activation energy is involved in the molecular adsorption of hydrogen, very fast kinetics of the adsorption and desorption process is achieved [22].

In chemisorption, (atomic adsorption, binding energy more than 2–3 eV (192.5–288.7 kJ/mol)), atoms of hydrogen create chemical bonds with the carbon. Hydrogen trapping states on carbon materials originate from covalent C–H interaction [27].

As the strength of the interaction between hydrogen and adsorbent materials increases, molecular hydrogen tends to dissociate into atomic hydrogen and subsequently diffuse into the adsorbents. This phenomenon is called spillover effect [22], which will be discussed in detail in 3rd section.

Activated carbon, graphene, fullerene, carbon nanofibers and carbon nanotubes could be sorted as the substrate carbon materials for hydrogen adsorption.

2.2.3.1. Activated carbons (ACs)

Bulky carbon with high surface area, the so-called activated carbon, is carbon structure able to absorb hydrogen in its microscopic pores. The main problems are that only some of the pores are small enough to catch the hydrogen atom and that high pressure must be applied in order to get the hydrogen into the pore. At 77K and 35 bars, system's storage density of 26 kg/m³ and 5.8 wt. % could be achieved [27].

Most of studies related with AC's are focused on the optimization of surface area via both experimental studies [2, 28] and computer modelling [29] to improve adsorption capacity. Zhao et al. reported that one of the highest storage performances (i.e. 6.6 wt. % at 77 K and 4 MPa) was achieved by KOH activation [28].

2.2.3.2. Graphite nanofibers (GNFs)

Graphite nanofibers consist of catalytically produced graphene sheets that are oriented to form various fibrous structures. The specific surface areas (BET) of these crystalline solids are normally between 100 and 300 m²/g but can sometimes reach values, up to 700 m²/g [1].

According to the review paper that presented by Ströbel et al. [1], most significant results have been obtained from with herringbone and platelet GNFs, up to 67,55wt.% hydrogen uptake capacity. These studies are interesting due to occurring ambient temperature alongside of having very high adsorption ratios.

2.2.3.3. Single Walled Carbon Nanotubes (SWNTs)

The hydrogen storage on single-walled carbon nanotubes is discussed in 3rd chapter in depth.

3. SINGLE-WALLED CARBON NANOTUBES

It is already admitted that the big bang of this chemical evolution began with investigation of multiwall carbon nanotubes by Lijima in 1991 [29], two years later Lijima discovered single wall carbon nanotubes [30].

With the Young's modulus of 1000 GPa, tensile strength of 30 GPa, electrical conductance higher than copper and thermal conductivity equivalent to diamond, SWNT have been at the centre of intensive and extensive interest all over the world qua the ultra-lightweight and ultra-strong material of the future [31]. Carbon nanotubes have attracted much expectation to store hydrogen because they have cylindrical structures that enhances curvature effect.

3.1. Structure of Single-Walled Carbon Nanotube

Single wall carbon nanotubes can be described as a one dimensional unit cell formed by rolling an infinite sheet of graphene with a chiral angle of θ , having one atom thick wall, within diameter size distribution of 1-2 nm [31]. SWNTs generally exist in the hexagonal structure bundles which are bonded to each other by Van der Waals bonds and can have 100-500 SWNTs [32].

Carbon nanotubes can be classified as arm chair, zigzag and chiral according to their crystal structures presented with (n,m) values. (n,0) nanotube with a chiral angle of 0° is called zigzag nanotube, (n,n) with a chiral angle of 30° is called armchair nanotube and if n is not equal to m and chiral angle is between 0° and 30° then it is called chiral nanotube [32].

3.2. Properties of Carbon Nanotubes

3.2.1. Chemical properties of carbon nanotubes

Curvature-induced pyramidalization and misalignment of the δ -orbitals of the carbon atoms induces a local strain and carbon nanotubes are expected to be more reactive than a graphene sheet [33].

3.2.2. Electrical properties of carbon nanotubes

Theoretical calculations [34] show that electrical properties of nanotubes depend on geometric structure. CNTs can be metals or semiconductors with different sized energy gaps, depending very sensitively on the diameter and chirality of the tubes.

SWNT's have two types of bonds due to sp^2 hybridization: the σ bonds, which are along the cylinder wall and form the hexagonal network; and the π bonds which interact between different tubes (Van-der Waals Force). Unexpectedly, σ bonds don't play an important role in the electronic properties because they are far away from Fermi level. In contrast, the binding and anti-binding π bands cross the Fermi level [35].

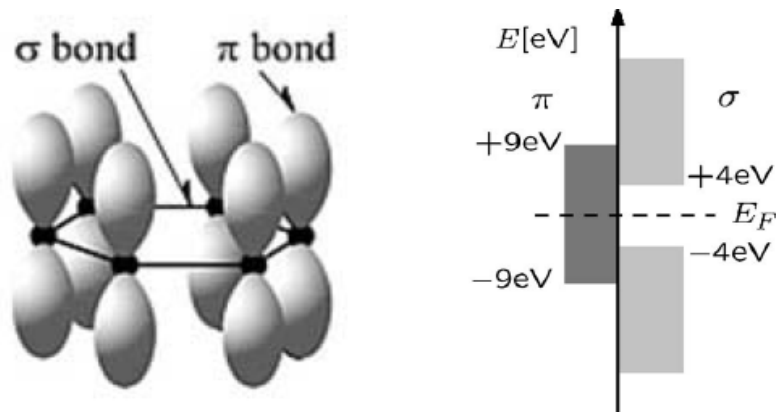


Figure 3.1 : Scheme of sp^2 hybridization in graphene; σ bonds, π bonds and their energies with respect to Fermi level [36]

Ab-initio pseudo-potential local density functional calculations [37] reveal that sufficiently strong hybridization effects can occur in small-diameter nanotubes which significantly alter their electronic structure.

3.2.3. Solubility of carbon nanotubes

Since carbon nanotubes are insoluble inherently, SWNT's can be functionalized via amidation and esterification of the nanotube-bound carboxylic acids.

Although solubility of carbon nanotubes is primary objective of functionalization, functionalization process of nanotubes came into this paper's domain in further discussions concerning the treatment of oxidized-defects via metal decoration to enhance hydrogen uptake capacity.

These solubilization functionalizations may roughly be divided into two categories: a direct attachment of functional groups to the graphitic surface and the use of the nanotube-bound carboxylic acids. It is reported that in various alcohol solvents, these functionalized SWNTs were solvated as individual tubes, making it possible to carry out further solution chemistry [38]. In the second category of functionalization reactions, the nanotube-bound carboxylic acids derived from intrinsic or induced defects. The latter refer to the creation of terminal carbons in the shortening of nanotubes, which are converted to carboxylic acids upon oxidation. One can see the schematic pathway of this process in Figure 3.2.

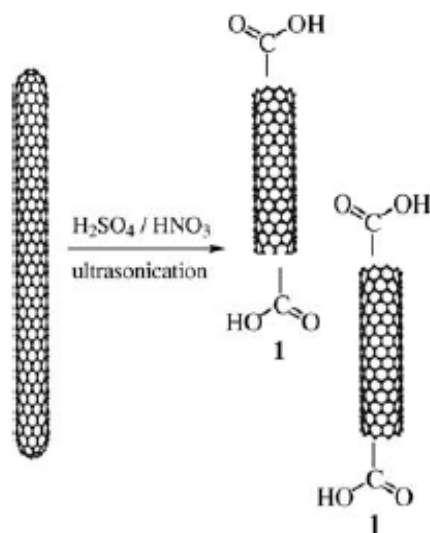


Figure 3.2 : Schematic representation of the oxidatively induced cutting and generation of carboxylic acid functionalities [38]

3.3. Purification of carbon nanotubes

As-synthesized CNTs prepared by arc-discharge, laser ablation or chemical vapor deposition (CVD) method inevitably contain carbonaceous impurities and metal catalyst particles. Carbonaceous impurities typically include amorphous carbon, fullerenes, and carbon nanoparticles [20]. Since the carbon source in arc discharge and laser ablation production method comes from the vaporization of graphite rods, some un-vaporized graphitic particles that have fallen from the graphite rods often exist as impurity in the final product. In addition, graphitic polyhedrons with enclosed metal particles also coexist with CNTs synthesized by arc discharge and laser ablation as well as high temperature (>1000 °C) CVD. Fullerenes can be easily removed owing to their solubility in certain organic solvents. Amorphous carbon is also relatively easy to eliminate because of its high density of defects, which allow it to be oxidized under gentle conditions [20], as well as could be purified via steam without destruction on nanotube tubular structure [39].

Metal impurities are usually residues from the transition metal catalysts. These metal particles are sometimes encapsulated by carbon layers making them impervious and unable to dissolve in acids [20]. Another problem that needs to be overcome is that carbonaceous and metal impurities have very wide particle size distributions and different amounts of defects or curvature depending on synthesis conditions, which makes it rather difficult to develop a unified purification method to obtain reproducibly high-purity CNT materials. To fulfill the vast potential applications and to investigate the fundamental physical and chemical properties of CNTs, highly efficient purification of the as-prepared CNTs is, therefore, very important.

Purification methods of CNTs can be basically classified into three categories: chemical, physical, and a combination of both.

3.3.1. Chemical oxidation

This method can effectively remove amorphous carbon and metal particles via selective oxidation except for those encaged in polyhedral graphitic particles. The high oxidative activity demonstrated by amorphous carbon is due to the presence of more dangling bonds and structural defects which tend to be easily oxidized; meanwhile the high reactivity of the CNPs can be attributed to their large curvature

and pentagonal carbon rings [18]. However it is knotty problem, especially for SWNTs, since graphitic particles have a similar oxidation rate to CNTs. In general, chemical oxidation includes gas phase oxidation (using air, O₂, Cl₂, H₂O, etc.), liquid phase oxidation (acid treatment and refluxing, etc.), and electrochemical oxidation. The disadvantages/advantages [40] (depending of application) of this method are that it often opens the end of CNTs, cuts CNTs, damages surface structure and introduces oxygenated functional groups (–OH, –C=O, and –COOH) on CNTs [22].

Tobias et al. claimed that gas phase purification via steam does not corrode the tubular structure of nanotubes and prevent from constitution of defects and functional groups on vacancies; just leaves behind clear SWNTs and metal catalyst particles, but removes the ends of SWNTs [39].

Hou et al. reported that neither HNO₃ treatment nor H₂O₂ oxidation followed by HCl rinsing is substantially efficient for removing both metal catalyst particles and carbon impurities without damaging tubular structures of SWNT. On the other hand, nitric acid treatment destroys SWNTs, leading to the production of carbonaceous impurities [18]. However, microwave-assisted inorganic acid treatment with HNO₃, HCl, and H₂SO₄ can rapidly dissolve metals efficiently without damaging the tube wall structure. It was indicated that with concentrated H₂SO₄/HNO₃ mixture (3:1), best results were achieved as 98% purity without decreasing the number of small diameter nanotubes [18].

It is hoped that liquid phase oxidation can be widely used for industrial application in the future considering the ability to eliminate impurities on a large scale. This method often leads to surface modification preferentially taking place on CNT sidewalls, which increases the chemical activity and the solubility of CNTs in most organic and aqueous solvents [38].

3.3.2. Physical Purification

To conserve the inherent physical and chemical properties of CNTs, purifications that do not involve oxidative treatment are highly desirable regarding morphology and physical properties of CNTs are different from impurities.

Among these, filtration depends on the solubility difference of SWNT and impurities in organic solvents; centrifugation can separate amorphous carbon and CNPs based

on the different stabilities in dispersions; high temperature annealing based on evaporating metal catalysts whilst other carbonaceous particles remain [20].

3.3.3. Multi-step purification

As mentioned above, gas phase oxidation is effective in removing amorphous carbon and polyhedral carbon at the cost of losing some CNTs but fails to remove a significant fraction of graphite particles and metal impurities. Liquid phase oxidation with strong oxidants is effective in removing carbonaceous impurities and metal particles simultaneously, whereas purified CNTs are always cut, opened and damaged. Physical purifications are effective in partly removing isolated carbonaceous or metallic impurities, while amorphous and spherical particles stuck to sidewalls or metal particles encapsulated in CNTs remain. In order to achieve desirable CNT purity with high yield, combinations of chemical and physical purifications are being intensely investigated. According to different needs, various kinds of multi-step purification methods are reported such as HIDE-assisted multi-step purification, Microfiltration in combination with oxidation, Sonication in combination with oxidation, High temperature annealing in combination with extraction [20]. Each of them was suggested to find a solution for own special conditions.

3.4. Functionalization of carbon nanotubes

The surface modification effect shows great potential for improving SWNT's physical and chemical properties for desired applications. The functionalization processes can be divided into two major classes: covalent or non-covalent, according to the nature of the bond between the functional group and the nanotube.

3.4.1. Non-covalent functionalization

An alternative strategy for preserving the intrinsic electronic and mechanical properties of CNTs consists in the non-covalent or supramolecular modification of CNTs. Such interactions primarily involve hydrophobic, van derWaals, and electrostatic forces, and require the physical adsorption of suitable molecules onto the sidewalls of the CNTs, whereas the hydrophobic part can enhance the solubility of CNTs or react with other molecules, alongside of ionic interaction of SWNTs

leading to the formation of acid–base salts or charge-transfer complexes. Non-covalent functionalization is achieved by polymer wrapping, adsorption of surfactants or small aromatic molecules, and interaction with porphyrins or biomolecules such as DNA and peptides [41].

Hauke and Hirsch reported that non-covalent functionalization does not produce defective sites on CNTs. Owing to their huge surface area, single-walled carbon nanotubes tend to aggregate into bundles very efficiently by van der Waals interactions [38].

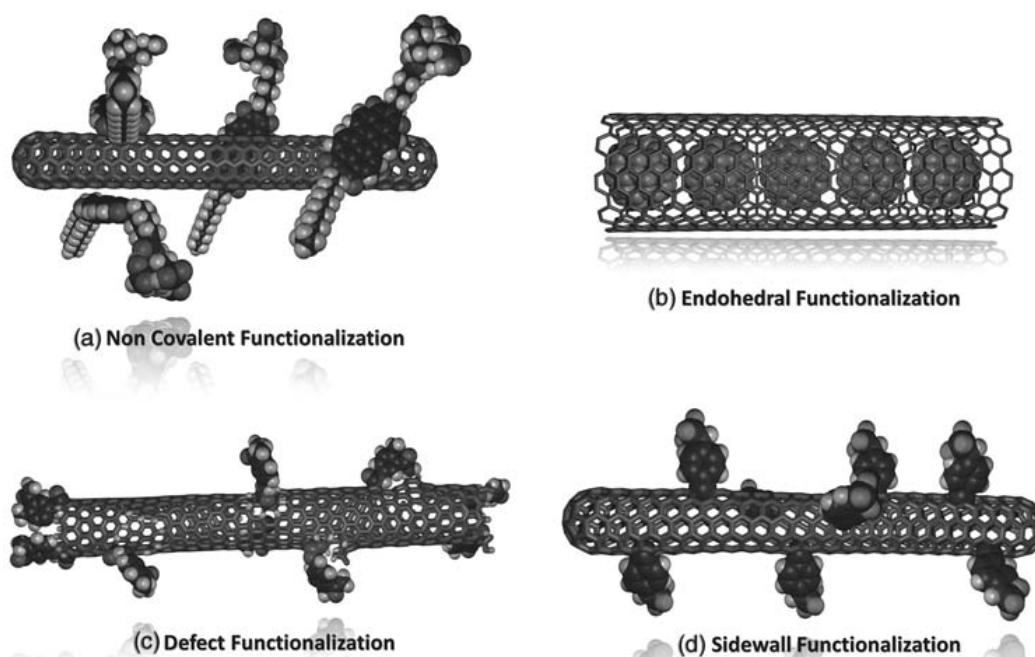


Figure 3.3 : Derivatization strategies for carbon nanotubes: (a)noncovalent exohedral functionalization with functional moieties based on specific CNT–molecule interactions (b)endohedral functionalization (C_{60} incorporation)(c) defect-group functionalization (d) direct covalent sidewall functionalization [38]

Beside this, it was overviewed that oxidized CNTs are easily dispersible in various amide-type organic solvents under the influence of an ultrasonic force field. In this sense, it was overviewed that the direct reaction of acid-purified short SWNTs with long-chain amines yielding very soluble zwitterionic materials likewise in Fig. 2.3(a) [42].

3.4.2. Covalent functionalization

As already expressed several times in purification step, this structural alteration can take place at the termini of the tubes and/or at the side walls as they are accepted highly favorable sites for oxidation. On the one hand, the direct sidewall functionalization in Fig 3.3(d) is associated with a re-hybridization of one or more sp^2 carbon atoms of the carbon network into a sp^3 configuration and a simultaneous loss of conjugation. On the other hand, the so-called defect functionalization sequence in Fig. 3.3(c) of CNTs is based on the chemical transformation of defect sites, intrinsically present or intentionally introduced by oxidation. Since province of study covered the hydrogen adsorption on oxidized surfaces, carboxyl/hydroxyl groups formed on the defects/vacancies upon oxidation will be main focus point, alongside of the metal doping.

Fig. 3.4 shows the main functional groups identified on CNT surfaces after the acid treatment. Among them, phenolic, lactonic, quinonic, and carboxylic groups are usually present in large amounts [43]

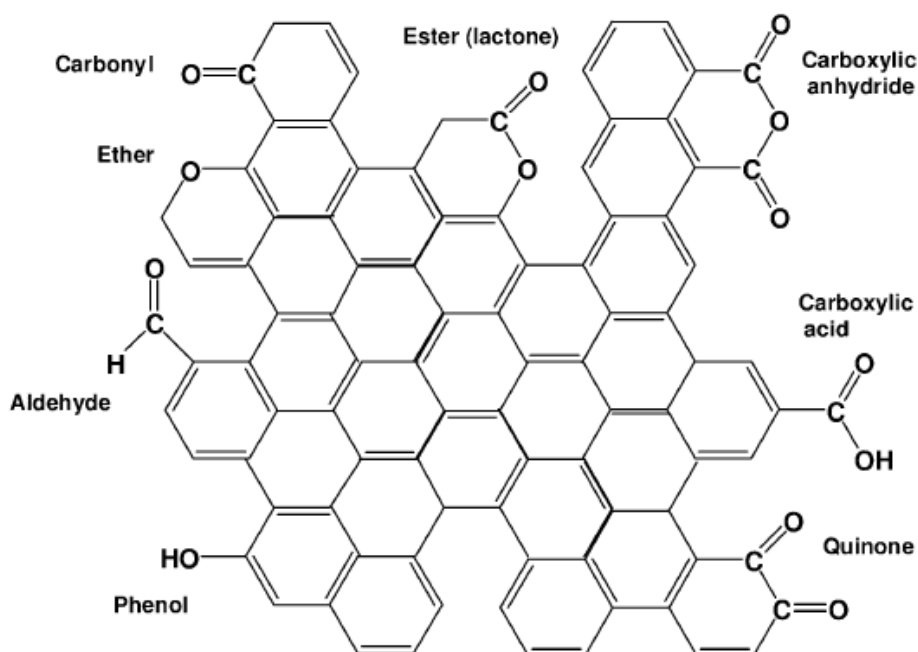


Figure 3.4 : Representation of the oxygen-containing surface groups on CNTs[43]

End functionalization does not dramatically change the chemical properties and also enhances the solubility in organic/inorganic solvents; as well as does not destroy the extended π -network, remaining the chemical and electronic properties [41, 44].

For identification of effect of chemical oxidants, SWNTs that was synthesized by CVD was oxidized by Zhang et al. via three kinds of oxidants: (1) HNO₃ (2.6 M), (2) a concentrated mixture of (3:1) H₂SO₄/HNO₃ and (3) KMnO₄.

(1) Refluxing in dilute HNO₃ introduces the carboxylic acid groups only at those initial defects that already exist [45].

(2) In contrast, sonication of SWNTs in H₂SO₄/HNO₃ increased the incidence of carboxylic acid groups not only at initial defect sites but also at newly created defect sites along the walls of SWNTs [45].

(3) Comparison to the two oxidants above, when KMnO₄ in alkali was used as the oxidant, which is relatively mild, different amounts of -OH, -C=O, and -COOH groups were introduced [45].

Gerber et al. [43] carried out molecular modelling study to analyse the reactivity of a vacancy. They dedicated that the elementary steps of carboxylic acid formation consist of: 1) the fast initial formation of carbonyl groups on the surface; 2) the final production of -COOH groups; and 3) the fact that previous investigations on grafting of -COOH did not concern the origin of the carbon atom at all.

In contrast to Gerber et al., density functional study carried out by Wang et al. [46] could be suggested to investigate the birth place of functional groups. They reviewed that in the oxidation, the carbon atoms in the -COOH groups mainly come from the nanotubes, except that the reaction starts by the attack on remaining CH and CH₂ groups that may be a residue of chemical vapor deposition at the initial stage (Fig 3.5).

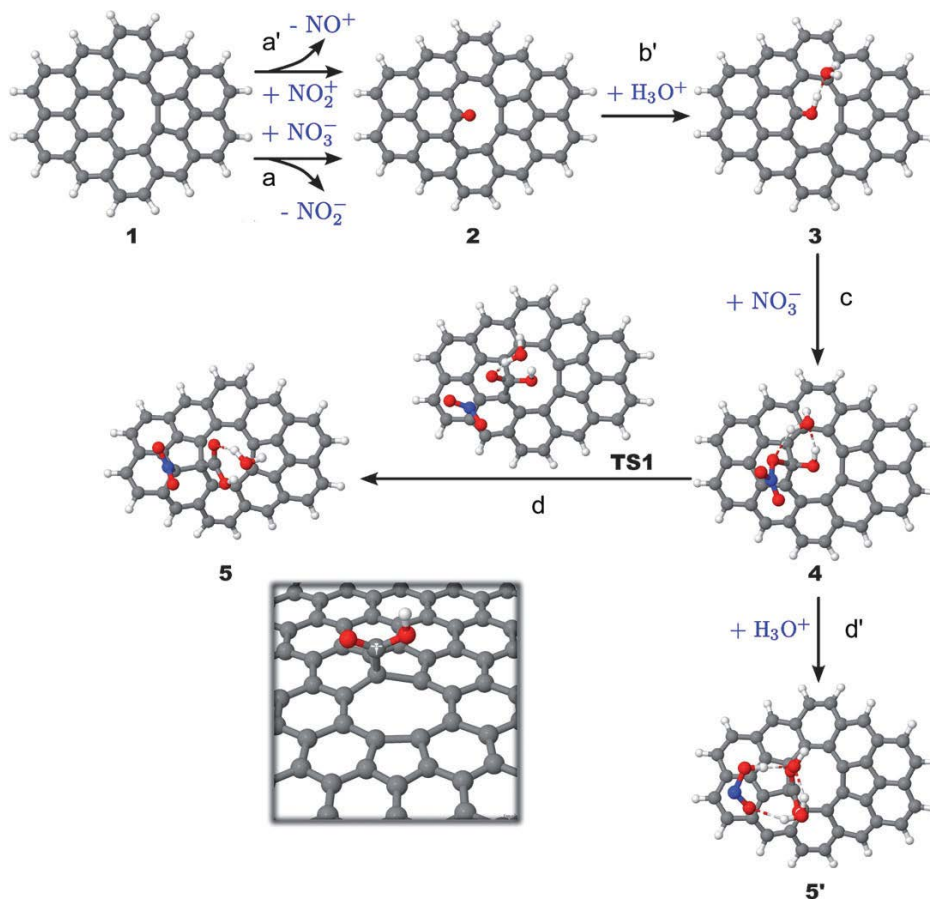


Figure 3.5 : Reactant (1), products (5 and 5'), transition state (TS1) and intermediates (2, 3, and 4) found on the proposed functionalization pathway of the model. The inset shows the -COOH functional group grafted on the di-vacancy formed on the graphene sheet at the end of the reaction [46]

3.5. Hydrogen adsorption on functionalized carbon nanotubes

The first study begins with Dillon et al.'s investigation of hydrogen storage capacity of non-purified of SWNT via thermal desorption spectroscopy. The investigation of purified carbon nanotubes having higher adsorption capacities than uncured ones led the researchers to investigate CNT surface chemistry, functionalization of carbon nanotubes in further studies [30].

Corresponding to visibility of hydrogen uptake enhancement with the presence of functionalized groups and/or metal doping on CNTs, experimental and theoretical publications were declared by several groups [12-17] and overviewed several times [1,2].

First of all, regarding the reason why defect sites are more favorable for adsorption site, characterization methods serve us to realize the root-cause behind the mechanism. Kamaras et al. and Itkis et al. revealed in their spectroscopic study that after acidic purification the doping will serve top in the Fermi level in the valance band, and the holes will behave as free carriers and produce strong adsorption in the far-IR. In other words, defects and vacancies occurred on CNT walls are more favorable sites for weak adsorption (physical adsorption) [44, 48].

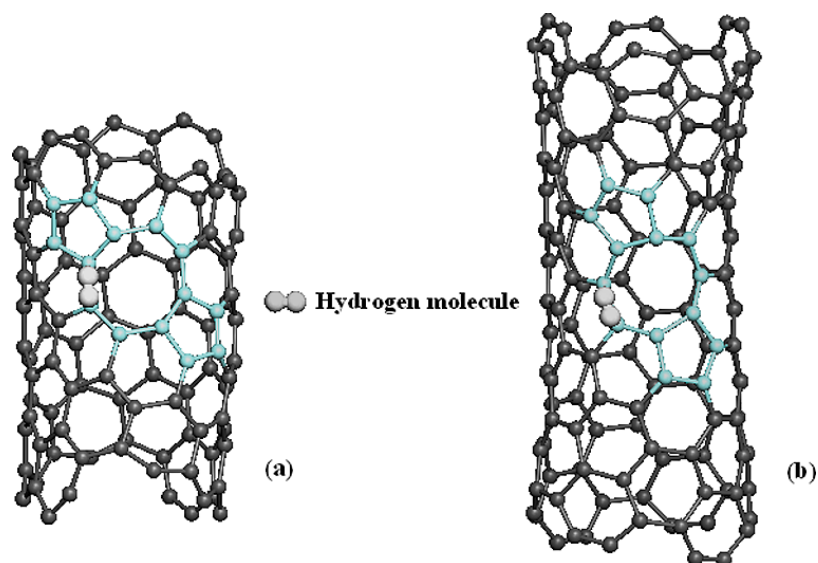


Figure 3.6 : Defected (a) (8,2) and (b) (6,4) nanotubes. Light colored portion indicates the presence of octagon and pentagons in the nanotube [17]

Corresponding to hydrogen uptake capacity, Gayathri et al. carried out DFT calculation on SWNTs with/without defect (.i.e grooves, interstitial channels, outer surface of bundle, and inner part pore) of the several chirality tubes such as armchair (5,5), zigzag (10,0) and chiral tubes (8,2) and (6,4)). For (8,2) tube their results show 50.54% increase in adsorption binding energy compared to defect free case while there is an increase of 55.84% for (6,4) tube. Similarly, 59.72% increase for defected (5,5) armchair tube and 36.84% increase for defected (10,0) zigzag semiconducting tube were observed (Fig. 3.6) [17].

Within the presence of functional group on CNT surface defects, H₂ adsorption in such hydrogenated/oxidized matrices is calculated by Volpe et al. via Grand Canonical Monte Carlo simulations. They investigated that the presence of

chemisorbed hydrogen generally reduces the gas-storage capability of carbon nanotubes[49].

It is very obvious theory that alkali (e.g. Li, K, etc.) or early transition-metal (e.g., Sc, Ti, and V) doped carbon nanotubes, fullerenes, and polymers have much attention for hydrogen storage applications at room temperature and ambient pressure. That is why several researchers have begun to head towards this type of functionalization for gas adsorption [50-56].

Taking into account of Kubas interaction (hybridization of the d states with the H_2 states), it was expected that these materials can enhance the interaction between the transition-metal element and H_2 , up to 0.2–0.6 eV [50]. The background of this logic is attributed to the contribution of unoccupied d levels of metal to the adsorption of the H_2 molecules via the hybridization of the d states with the H_2 states as in the case of H_2 binding to transition-metal atoms [50].

Lee et al. demonstrated the hydrogen adsorption mechanism and maximum capacity when several metals such as Ca, B, N were doped individually or conjugately on pristine, stone-wall defect and various type vacancies. In order to investigate the maximum intake capacity, clustering of Ca with hydrogen molecules on pristine and N-doped CNTs was carried out because of the small binding energy of Ca to the CNTs. They concluded that the gravimetric capacity of ~5 wt. % hydrogen was achieved by the binding of per hydrogen molecule with the energy of ~0.2 eV/ H_2 via the hybridization of the empty $Ca3d$ orbitals with the $H_2\sigma$ orbitals and clustering of Ca onto the defect sites of SWNT [50].

Moreover, Bhattacharya et al. [51], Yildirim et al. [52] and Shevlin et al. [53] surveyed similar DFT studies about hydrogen adsorption capacity with Ti doping except that Bhattacharya et al. preferred the Ti capping on endohedral and hexahedral surface of (6,6) BC_4N SWNT [51] whilst Yildirim et al. chose (8,0) defect-free SWNT [52] and Shevlin et al. selected (8,0) SWNT with/without vacancy defect [53]. Bhattacharya et al. [51] claimed that, at high Ti coverage, the system can absorb up to four hydrogen molecules per Ti atom (5.6 wt.% hydrogen uptake) with successive energies of adsorption lying in the range of ~0.4-0.7 eV. Four years before Bhattacharya et al.'s, Yildirim et al. [52] affirmed that Ti doped (8,0) defect free SWNT can bind four hydrogen molecules for per Ti atom with the binding

energy of -0.83 eV, 0.45 eV/H₂, 0.34 eV/H₂ respectively with the increasing number of hydrogen molecule. Incidentally, during the adsorption of first hydrogen molecule, a special mechanism, that is called spillover, has been observed. Spillover has been proposed as a general mechanism to enhance the storage density of carbon-based nanostructures. This approach relies on the use of a metallic catalyst to dissociate molecular hydrogen, using surface diffusion through a bridge to store atomic hydrogen in a receptor [1, 22, 26, 52, 54-56]. Hereupon, it can be suggested that the hydrogen binding on a doped metal is an unusual combination of chemisorption and physisorption [52]. Shevlin et al. [53] indicated in addition to Yildirim et al. [52] that vacancy capped with Ti is highly favorable, that also prevents nanoparticles coalescence. The defect-modulated Ti system can adsorb five H₂ molecules with binding energies in the range from -0.2 eV to -0.7 eV/H₂. That means, at full coverage of Ti on nanotube lead to adsorb of 7.1 wt.% hydrogen stably at room temperatures [53].

4. COMPUTATIONAL METHODS

Computational chemistry and physics are used in a number of different ways. Although computational models may not be perfect, they are often good enough to rule out compounds as being unsuitable for their intended use. This is very useful information because synthesizing a single compound could require months of labor and raw materials, and generate toxic waste. A second use of computational chemistry and physics is to understand the physical phenomena at the atomistic level. There are some properties of a molecule that can be obtained computationally more easily than the experiments. There are also insights into molecular binding, which can be obtained from the results of computations that cannot be obtained from any experimental method. Thus, many experimental chemists and physicists are now using computational modelling tools to gain additional understanding of the compounds being examined in the laboratory.

4.1. Density Functional Theory

Density Functional Theory (DFT) is a quantum mechanical modelling method in which the energy of a molecule can be determined from the electron density instead of a wave function. The theorem that originally suggested by Hohenberg and Kohn applied only to finding the ground-state electronic energy of a molecule. A practical application of this theory was developed and formulated by Kohn and Sham. In this formulation, the electron density is expressed as a linear combination of basic functions. A determinant is then formed from these functions, called Kohn-Sham orbitals. In order to compute the energy, the electron density obtained from this determinant of orbitals is used[57].

Before rummaging density functional theory, some basic definitions must be clarified. The Schrödinger equation could be accepted a preliminary definition for solving an associated eigen-value in which satisfies time-dependant and non-relativistic eigen-value equation [58].

$$H\Psi_i(\vec{x}_1, \vec{x}_2, \dots, \vec{x}_N, \vec{R}_1, \vec{R}_2, \dots, \vec{R}_M) = E_i\Psi_i(\vec{x}_1, \vec{x}_2, \dots, \vec{x}_N, \vec{R}_1, \vec{R}_2, \dots, \vec{R}_M) \quad (4.1)$$

in this equation, H is the Hamiltonian operator and ψ is a set of solutions, or eigenstates, of the Hamiltonian.

If the problem does not have any time dependence, the time-dependent Schrödinger equation can be reduced to the time-independent Schrödinger equation. The atomic systems we model consist of nuclei and electrons, and the first step before calculating the electronic structure is to apply the Born-Oppenheimer approximation to decouple the nuclei and the electrons. When this is done, nuclei can be treated as fixed external potential and minimize the energy of the electronic system in this potential. Within the Born-Oppenheimer approximation the electrons are described by the Hamiltonian acting on a many-body wave function that contains all about the electronic state[59].

In this respect, the detailed definition of the Hamiltonian depends on the physical system being described by the Schrödinger equation [59].

$$\hat{H} = \sum_{i=1}^N \frac{1}{2} \nabla_i^2 + \sum_{i=1}^N v(r_i) + \sum_{i<j}^N \frac{1}{|r_i - r_j|} \quad (4.2)$$

The Hamiltonian equation (Eq. 4.2) can be split into the kinetic energy, the interaction with the external potential, and electron-electron interaction, respectively.

4.1.1. Hohenberg and Kohn's theorem

Hohenberg and Kohn's first theorem states that the ground-state electron density uniquely determines all properties, including the energy and wave function, of the ground state. It means that we can think about solving the Schrödinger equation by finding a function of three spatial variables, the electron density, rather than a function of $3N$ variables, the wave function. However, although the first Hohenberg–Kohn theorem rigorously proves that a functional of the electron density exists that can be used to solve the Schrödinger equation, the theorem says nothing about what the functional actually is. The second Hohenberg–Kohn theorem defines an important property of the functional: The electron density that minimizes the energy of the overall functional is the true electron density corresponding to the full solution of the Schrödinger equation. If the “true” functional form were known, then the

electron density could be varied until the energy from the functional is minimized, that gives a prescription for finding the relevant electron density [58].

4.1.2. Kohn Sham's theorem

In DFT the many-body wave function is replaced by the ground state electron density. One simply utilize the fact the electrons satisfy the Schrödinger equation, and therefore it is sufficient to know their preferred density at 0K to know everything about the system.

Kohn Sham showed that the task of finding the right ground state electron density can be expressed in a way that involves solving a set of equations in which each equation only involves a single electron [58].

$$\underbrace{\left[\frac{\hbar^2}{2m} \nabla^2 + V(r) \right]}_{\text{I}} + \underbrace{V_H(r)}_{\text{II}} + \underbrace{V_{XC}(r)}_{\text{III}} \psi_i(r) = \varepsilon_i \psi_i(r) \quad (4.3)$$

I: the interaction between an electron and the collection of atomic nuclei

II: Hartree potential describes the total electron density defined by all electrons in the problem

III: exchange-correlation contributions to the single electron equations

The iterative pathway is suggested for rational calculation of theorem could be set as definition of an initial, trial electron density; solving the Kohn–Sham equations defined using the trial electron density to find the single-particle wave functions; calculation of the electron density defined by the Kohn–Sham single particle wave functions, and comparison of old and new electron density. If the two densities are the same, then this is the ground-state electron density, and it can be used to compute the total energy. If the two densities are different, then the trial electron density must be updated in some way. Once this is done, Kohn–Sham could be solved by this true electron density to evaluate the final ground-state electron density in further step [58, 60].

The inexplicit part of Eq. (4.3) is exchange-correlation potential since it cannot be initially imported. In order to overcome this part, the exchange–correlation potential at each position is set to be equal to the known exchange–correlation potential from

the uniform electron gas at the electron density observed at that position. This approximation uses only the local density to define the approximate exchange–correlation functional, so it is called the local density approximation (LDA). The LDA gives us a way to completely define the Kohn–Sham equations, but it is crucial to remember that the results from these equations do not exactly solve the true Schrödinger equation because the true exchange–correlation functional are not used [58, 59, 61].

The best known class of functional after the LDA uses information about the local electron density and the local gradient in the electron density; this approach defines a generalized gradient approximation (GGA). Since GGA includes more physical information than the LDA, that will influence to be taken under consideration. Two of the most widely used functionals in calculations involving solids are the Perdew–Wang functional (PW91) and the Perdew–Burke–Ernzerhof functional (PBE) [58]. Among them, RBE functional is the most widely-used one because it gives good results for molecular binding to transition metal surfaces [61].

4.1.3. Reciprocal space and k points

In any approach, the essential point is to define the locations of all atoms in unit cell, which is also called primitive cell. A more general way of thinking about the primitive cell is that it is a cell that is minimal in terms of volume but still contains all required information to fully define a periodic material with infinite extent [58]. Let us assume that a unit cell is defined as a three-dimensional space cube with the side length of a . That is, the positions of all atoms are defined using normal three-dimensional Cartesian coordinates by

$$r = (n_1 a, n_2 a, n_3 a) \quad (4.4)$$

for any integers n_1 , n_2 , and n_3 . A much more common crystal structure in the periodic table is the face-centred-cubic (fcc) structure [58]. The primitive cell for the fcc metal can be defined by connecting the atom at the origin in the structure defined above with three atoms in the cube faces adjacent to that atom. That is, we define cell vectors:

$$a_1 = a(k, l, 0) \quad a_2 = a(0, m, n) \quad a_3 = a(r, 0, s) \quad (4.5)$$

k, l, m, n, r and s are the real numbers.

These vectors define the fcc lattice if atoms are placed at positions;

$$\mathbf{r} = n_1 \mathbf{a}_1 + n_2 \mathbf{a}_2 + n_3 \mathbf{a}_3 \quad (4.6)$$

for all integers $n_1, n_2,$ and n_3 .

Just as we defined positions in real space in terms of the lattice vectors $\mathbf{a}_1, \mathbf{a}_2,$ and $\mathbf{a}_3,$ it is useful to define three vectors that define positions in reciprocal space. These vectors are called the reciprocal lattice vectors, $\mathbf{b}_1, \mathbf{b}_2,$ and \mathbf{b}_3

$$\mathbf{b}_1 = 2\pi \frac{\mathbf{a}_2 \times \mathbf{a}_3}{\mathbf{a}_1 \cdot (\mathbf{a}_2 \times \mathbf{a}_3)} \quad \mathbf{b}_2 = 2\pi \frac{\mathbf{a}_1 \times \mathbf{a}_3}{\mathbf{a}_2 \cdot (\mathbf{a}_1 \times \mathbf{a}_3)} \quad \mathbf{b}_3 = 2\pi \frac{\mathbf{a}_1 \times \mathbf{a}_2}{\mathbf{a}_3 \cdot (\mathbf{a}_1 \times \mathbf{a}_2)} \quad (4.7)$$

As primitive unit cell is already expressed of that definition, second major duty is to generate the solution as periodic in finite space. In such a case, to use the Bloch's theorem will serve to achieve the periodicity [58, 61].

$$\Phi_{\mathbf{k}}(\mathbf{r}) = \exp(i\mathbf{k} \cdot \mathbf{r}) u_{\mathbf{k}}(\mathbf{r}) \quad (4.8)$$

The space of vectors \mathbf{r} is called real space, and the space of vectors \mathbf{k} is called reciprocal space (or simply \mathbf{k} space). The idea of using reciprocal space is so central to the calculations.

Consequently, the main objective all these transformations is to create a primitive cell in reciprocal space; it is also addressed as *Brillouin zone* (BZ). The Brillouin zone plays a central role in the band theory of materials [58].

4.1.4. The Energy cut-off and pseudopotentials

In eq. (4.8), $u_{\mathbf{k}}(\mathbf{r})$ term represents of the periodic part that can be expanded in terms of a special set of plane waves with the same periodicity as the supercell.

$$u_{\mathbf{k}}(\mathbf{r}) = \sum_{\mathbf{G}} c_{\mathbf{G}} \exp[i\mathbf{G} \cdot \mathbf{r}] \quad (4.9)$$

where the summation is over all vectors defined by

$$\mathbf{G} = m_1 \mathbf{b}_1 + m_2 \mathbf{b}_2 + m_3 \mathbf{b}_3 \quad (4.10)$$

with integer values for m_i and the reciprocal lattice vectors, b_1 , b_2 , and b_3 that were already defined above.

With the substitution of eq. (4.9) into eq. (4.8), the general solution of Bloch's theorem (Eq. 4.11) is evaluated at even a single point in k space involves a summation over an infinite number of possible values of G .

$$\Phi_k(\mathbf{r}) = \sum_{\mathbf{G}} c_{\mathbf{k}+\mathbf{G}} \exp[i(\mathbf{k} + \mathbf{G})\mathbf{r}] \quad (4.11)$$

Since the purpose of the matter is to evaluate the solutions with lower energies than the solutions with higher energies, the interpreted infinite sums that driven from above must be truncated to include only solutions with kinetic energies. If the cut-off energy is assigned as below,

$$E_{cut} = \frac{\hbar^2}{2m} G_{cut}^2 \quad (4.12)$$

the infinite sum then reduces to

$$\Phi_k(\mathbf{r}) = \sum_{|\mathbf{G}+\mathbf{k}| < G_{cut}} c_{\mathbf{k}+\mathbf{G}} \exp[i(\mathbf{k} + \mathbf{G})\mathbf{r}] \quad (4.13)$$

In most cases, a default cutoff energy is assigned for each element and the largest cutoff energy for any of the atoms in the supercell is assigned as the overall cutoff energy [58].

The most important approach to reducing the computational burden due to core electrons is to use pseudo-potentials. In the pseudo-potential method the nuclei potentials and core electrons are replaced with soft pseudopotentials. This replacement is accompanied by a replacement of the true valence wave functions with pseudo wave functions. The drawback of pseudo-potential brings a minimum energy cutoff that should be used in calculations including atoms associated with that pseudo-potential in contrast to above expression that how much the cut-off energies are assigned higher so that the convergence of the solution is enhanced. Pseudopotentials requiring high cutoff energies are said to be hard, while more computationally efficient pseudo-potentials are carried out with low cutoff energies [58, 61].

5. RESULTS AND DISCUSSION

5.1. Computational Setup

All electronic structure calculations were carried out using DACAPO plane wave code [62], with a cutoff energy of 340 eV (for the density grid a cutoff of 500 eV has been employed). The RPBE [62] exchange-correlation functional was utilized. In DACAPO, the ionic cores are described by ultrasoft pseudopotentials [63]. The electronic Brillouin zones were sampled with $(1 \times 1 \times 3)$ k -points. Structural optimizations were ended when all forces are smaller than 0.03 eV \AA^{-1} using a quasi-Newton method (BFGS) [64] within the atomistic simulation environment [65]. The calculations in (8,0) nanotube were carried out in a orthorhombic cell with $21.3 \text{ \AA} \times 16.3 \text{ \AA} \times 8.54 \text{ \AA}$. This selection of cell parameters resulted a separation of 10 \AA between carbon atoms on adjacent nanotubes along the a and b directions.

5.2. Defect Generation and Hydrogen Adsorption

5.2.1. Defect generation and oxidative functionalization

The whole calculations were carried out using a zigzag (8,0) SWNT containing 64 carbon atoms in the unit cell as shown in Fig. 5.1.

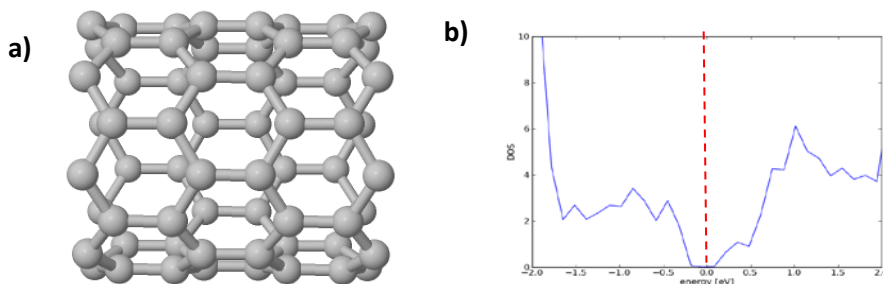


Figure 5.1 : a) Plane(8,0) zigzag SWNT b) DOS. Fermi level is indicated with red dashed line.

The Fig 5.1b shows the density of states (DOS) of pristine calculated using $(1 \times 1 \times 16)$ Monkhorst-Pack k points. It is known that CNT's can be either metallic or

semiconductor depending on their diameter and chirality. (8,0) zigzag SWNT is a semiconductor with an energy gap around the Fermi level.

In this study, it is assumed that side-wall defect was occurred during the purification via chemical oxidation. It is experimentally [66] known that following the purification of SWNT via chemical oxidation, the side-wall defects were obtained preferably on the sidewalls with the higher fraction than on the tube ends. In order to create an oxidized SWNT defect, first an atomic vacancy must be formed in the SWNT. This can simply be performed by removing a carbon atom from the nanotube as indicated in Figure 5.1. Upon the vacancy formation, three hexagonal rings were transformed into a pentagon and distorted octahedron after relaxation. In case of atomic vacancy in the hexagonal rings, three dangling bonds (DB) are created indeed. As Wang et al. declared [40], one of them creates binding with $-\text{COOH}$ group during carboxylic functionalization due to dandling bonds more energetically preferable than unharmed ones, and the rest DBs prefer to recombine each other. In this context, the configuration owing newly formed C-C bond -producer of pentagonal- perpendicular to the tube axis is more energetically stable than two other possibilities. The following formula has been employed to calculate the vacancy formation energy:

$$E_{f,vacancy} = E_{cell\ with\ (n-1)\ atomsonnsites} - \frac{n-1}{n} E_{perfect} \quad (5.1)$$

Here, $E_{f,vacancy}$ is the vacancy formation energy and it is obtained as the energy difference between one atom missing cell ($E_{cell\ with\ (n-1)\ atomsonN\ sites}$) and the perfect cell ($E_{perfect}$). This vacancy energy was calculated to be 5.32 eV and it is in very good agreement with the theoretically found value (5.54 eV) [40] and experimental one found by Lu and Pan [67].

DOS and partial density of states (PDOS) calculations shown in Fig 5.2b indicates that vacancy formation changes the whole electronic properties of (8,0) SWNT. The presence of vacancy breaks the symmetry of the system and creates available states around the Fermi level and those filled by electrons in contrast to pristine.

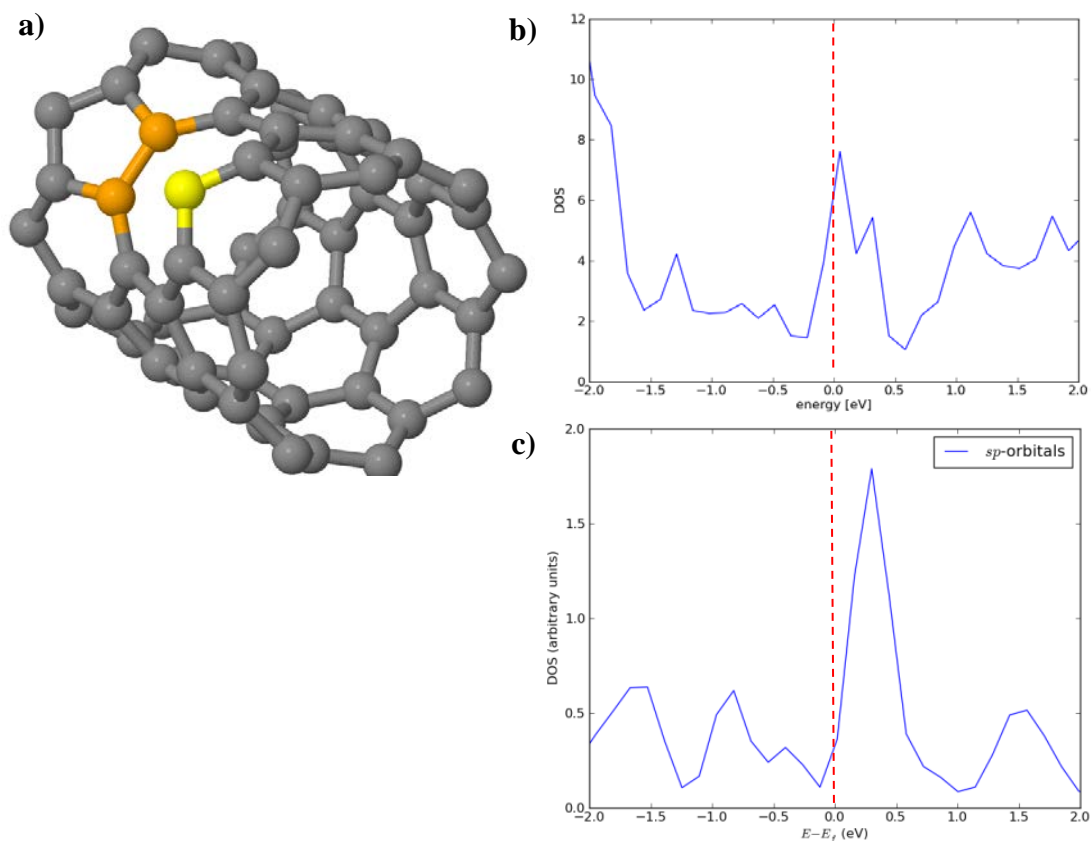


Figure 5.2 : a) SWNT having single vacancy on sidewall. b) DOS of the whole system. c) PDOS of carbon atom shown as yellow. Two dangling carbon atoms are indicated with orange. Fermi level is indicated with the red dashed line.

Following the vacancy creation, carbon site shown in yellow in Fig. 5.2a was oxidized (with -OOH) SWNT was used in the computations. The relaxed corresponding structure using the plane wave DFT method is shown in Figure 5.3a. During the geometry optimization, the direction of COOH group was rotated along the tube axis. A similar orientation was also found by Wang et al. [40].

Furthermore, they also investigated another possible conformation of oxidized SWNT in which the position of the pentagon is tilted toward the tube axis. They found that the configuration which is the same as ours has a total energy of 0.55 eV lower than other one. Therefore, in the current study, only the most stable structure was used for all computations. In the oxidized SWNT configuration, the C-COOH bond is tilted upwards from the SWNT axis with an angle of approximately 56° and hence the tube takes an oval shape. Moreover, the formed CCO and OCO angles are 125.5° , 112.9° and 121.6° , respectively.

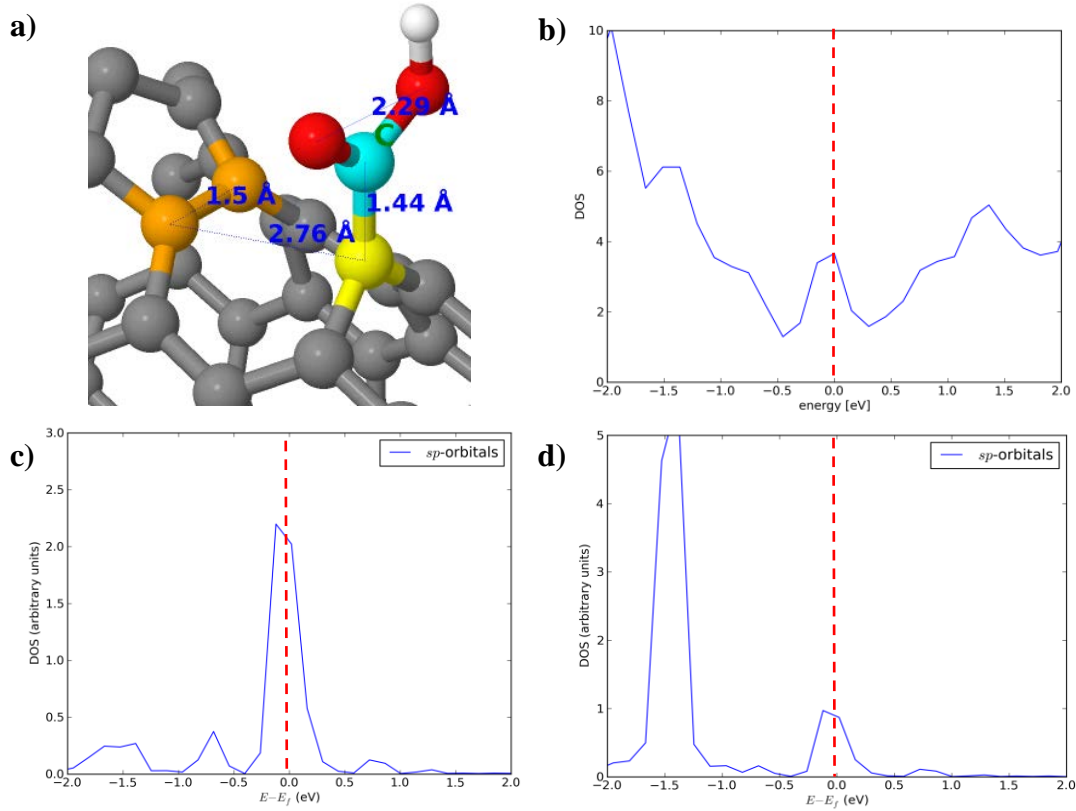


Figure 5.3 : **a)** The relaxed vacancy defect oxidized (8,0) SWNT. **b)** DOS of the whole system. **c)** PDOS of carbon atom indicated with yellow. **d)** PDOS of COOH group. Representing colors: carbon: grey; oxygen: red; hydrogen: white. Two dangling carbon atoms are indicated with orange. Fermi level is indicated with red dashed line.

Our results demonstrated that when an atomic vacancy is created, the two dangling carbon atoms tend to create a binding so as to form a pentagonal ring. In our results, dangling bond was created with 1.50\AA binding distance after structural relaxation while initial space was 1.98\AA . It is obvious from Fig. 5.3a that $-\text{OOH}$ group pulls out the carbon atom, to which the $-\text{OOH}$ group is bound, from the tube axis. The distance from this carbon atom to the nearest carbon atom on the tube is 1.44\AA . Due to this new arrangement, the shortest distance between the nearest carbon atom to which COOH group is bound and the carbon atoms on the pentagon is 2.76\AA and 2.29\AA .

5.2.2. The hydrogen adsorption on oxidized SWNT

Pure SWNT binds loosely the hydrogen. Therefore, vacancy creation and metal decoration in SWNT's might improve their hydrogen storage capabilities. Gaythri et al. [17] recently calculated the hydrogen binding energy on pure SWNTs. They considered (5,5), (10,0), (8,2) and (6,4) SWNTs and calculated the binding energies to be 0.26, 0.26, 0.24 and 0.26 eV, respectively. They also found that hydrogen prefers an alignment perpendicular to the hexagon of the tube (at least 5.78 Å away from the tube). Creating vacancies, however, did not dramatically change the binding energies of hydrogen only the distance between hydrogen and the tube was shortened at most to 5.23 Å. In order to see the effect of oxidization to binding, first the binding energy of hydrogen on the oxidized SWNT has been investigated. In these computations, the binding energy of hydrogen cohesive energy is calculated using the following formula;

$$E_{\text{ads}} = E_{\text{CNT}+\text{H}_2} - (E_{\text{CNT}} + E_{\text{H}_2}) \quad (5.2)$$

where, E_{ads} is the binding energy of hydrogen on SWNT and E_{CNT} , E_{H_2} and $E_{\text{CNT}+\text{H}_2}$ are the total energies of SWNT, H_2 and $\text{SWNT}+\text{H}_2$, respectively.

There are many available sites where the hydrogen or metal atom can be adsorbed on the oxidized SWNT's as shown in Fig. 5.4. The considered unitcell of oxidized SWNT's has been divided into three regions, designated as 11x, 12x and 13x (x is a integer number in the range of 1-5), each containing a hexagon. Here, the second and third digits represent general and explicit adsorption site on the tube. In the (8,0) SWNT's, there are 8 hexagons in total on the surface of the tube and 5 of them are non-equivalent. Actually, these non-equivalent hexagons are represented with the third digit, x. Since the surface of tube is changed upon the oxidization with the removal of 2 hexagons, there are only 3 non-equivalent adsorption site on the surface of the tube where the oxidation occurs. Therefore, in total, there are 13 unique adsorption sites.

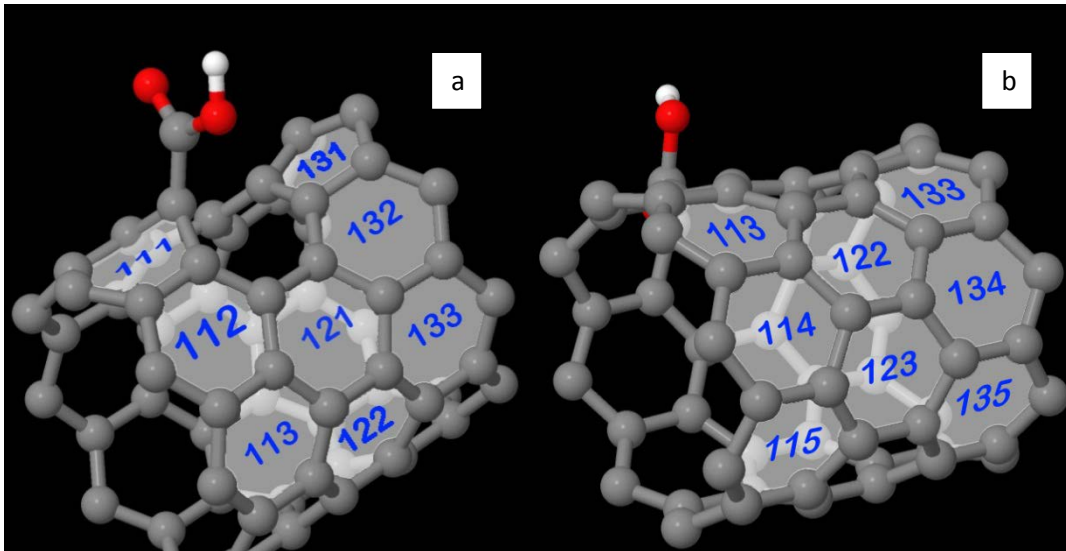


Figure 5.4 : Adsorption sites on the oxidized SWNT

The most dramatic effect to hydrogen binding should be at the adsorption sites which are very close to $-OOH$ group. Therefore, first (131) and (111) sites have been considered to investigate the hydrogen binding in the oxidized SWNT's. On (131) site, a hydrogen molecule was initially set in front of carboxyl group with distance of 2.1\AA away from oxygen and 2.46\AA away from the nearest carbon atom. Similarly, for the 111 adsorption site, the corresponding distances are 2.45\AA and 2.19\AA , respectively. Using the equation 19, the calculated binding energies in these sites were obtained to be -0.022 eV and -0.005 eV , respectively. Additionally, a hydrogen molecule was also placed just above the $-OOH$ group. This orientation gave a very low binding energy, -0.005 eV . These results show that hydrogen cannot bind to these sites.

Then, the binding of hydrogen is investigated at the sites which are at the opposite direction of (111) and (131). These sites are (115) and (135) being furthestmost ones from the $-OOH$ group. Similar to (111) and (131), a very weak binding energy was calculated for the (115) and (135) sites, which were -0.006 eV and -0.005 eV , respectively. All the optimized geometries and corresponding binding energies were shown in Fig. 5.5 and Table 5.1.

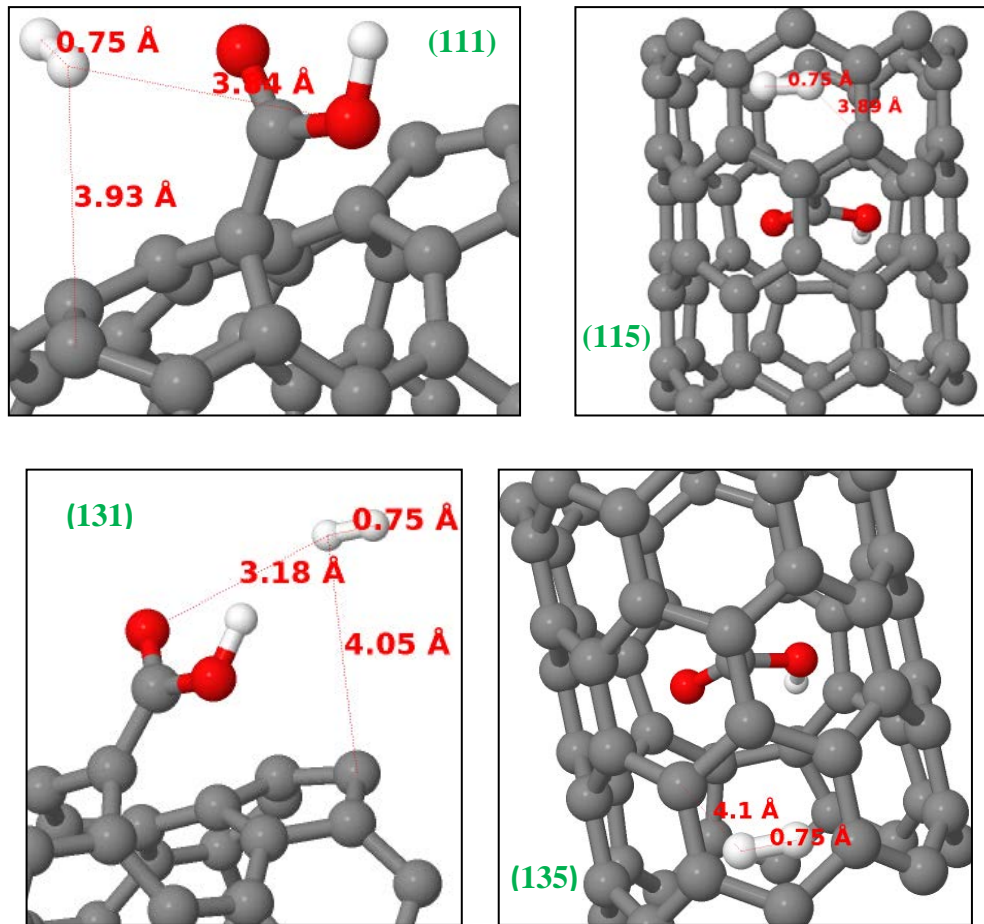


Figure 5.5 : Adsorption of hydrogen on (111), (115), (131) and (135) sites of the oxidized SWNT

Table 5.1 : Binding energies of hydrogen molecules on (111), (115), (131) and (135) sites of the oxidized SWNT.

Adsorption sites	Binding energies [eV]
Above -OOH	-0.005
(111)	-0.010
(115)	-0.006
(131)	-0.022
(135)	-0.005

In particular, the effect of molecular axis configuration of hydrogen molecule has been examined with respect to the found results of Gaythri et al. [17] and Ye et al. [68]. Except of above -OOH and (115) cases, none of relaxed structures in perpendicular hydrogen axis configuration has lower energies than the horizontal hydrogen axis configuration. 0.007 eV attenuation has been observed in the cohesive energies of hydrogen molecule for (111) and (131) position. On (111), hydrogen

molecule was relaxed 0.67 Å closer to the nearest carbon atom and 0.24 Å closer to the carbon of COOH in parallel axis to titled COOH. On (131), in contrast to (111) hydrogen molecule has been relocated farther with 0.34 Å to dangling oxygen and 0.11 Å to the nearest carbon in hexagonal ring. For (135), hydrogen molecule was relocated perpendicularly 0.5 Å closer to the nearest carbon in hexagonal ring and bonded 0.022 eV weaker onto the hexagonal ring conversely. Above –OOH group, hydrogen molecule was bonded 0.0076 eV stronger and relocated perpendicularly 0.12 Å further from the dangling oxygen than the horizontal relocated one. In contrast to the study of Gaythri et al. [17], hydrogen molecules were bonded perpendicularly/horizontally on the hexagonal carbon ring of plane side of SWNT with the distance interval of 3.5-4 Å to the nearest carbon; 2 Å closer at least than Gaythri et al.'s results. It could be attributed to the (8,0) defect free SWNT owing higher curvature than (10,0) defect free SWNT.

5.3. Hydrogen adsorption on metal doped, oxidized SWNTs

As indicated in section 5.2.2, hydrogen is weakly bound to the SWNT surface. Actually, a promising hydrogen storage material should adsorb hydrogen not too weakly or too strongly. Weak binding means, there is no interaction between hydrogen and the surface. Therefore, hydrogen can easily leave the surface. On the other hand, a strong binding is also not a target, since more energy is required to desorb the hydrogen from the surface, which ultimately limits the practical use of the material. What we are searching for materials moderately binds the hydrogen. This binding energy gap is 0.2 – 0.6 eV [50]. One way to reach this target using SWNT is to dope it with metal atoms. The M.Sc. thesis of Senyer [69], a screening study using 14 metal species indicated in Fig. 5.6, showed that it is really possible to obtain moderate binding between hydrogen and pure SWNT's. In the current study, the same metal species used in the screening.

Since there are 13 different adsorption sites and 14 metal types, it is not easy to carry out the all calculations. Therefore, first, the effect of adsorption site has been analyzed for only Ni and Ti metals.

19 K 39.098	20 Ca 40.078	21 Sc 44.956	22 Ti 47.867	23 V 50.942	24 Cr 51.996	25 Mn 54.938	26 Fe 55.845	27 Co 58.933	28 Ni 58.693	29 Cu 63.546	30 Zn 65.38
37 Rb 85.468	38 Sr 87.62	39 Y 88.906	40 Zr 91.224	41 Nb 92.906	42 Mo 95.96	43 Tc (98)	44 Ru 101.07	45 Rh 102.91	46 Pd 106.42	47 Ag 107.87	48 Cd 112.41
55 Cs 132.91	56 Ba 137.33	57-71 *	72 Hf 178.49	73 Ta 180.95	74 W 183.84	75 Re 186.21	76 Os 190.23	77 Ir 192.22	78 Pt 195.08	79 Au 196.97	80 Hg 200.59
87 Fr (223)	88 Ra (226)	89-103 #	104 Rf (265)	105 Db (268)	106 Sg (271)	107 Bh (270)	108 Hs (277)	109 Mt (276)	110 Ds (281)	111 Rg (280)	112 Cn (285)

Figure 5.6 : Selected metals

5.3.1. Ni and Ti doped oxidized SWNT's

To select the best adsorption site to be used in the screening study, binding of Ni and Ti atoms on 13 different sites have been calculated. In this respect, energy of the metal atoms is also required. For the computation of these values, metal atoms have been placed into a cubic cell with a cell parameter, $a = 10 \text{ \AA}$ and $(8 \times 8 \times 8)$ k -points have been employed. Binding energy results obtained for Ni and Ti are given in Table 5.2. It is clear that the binding site preference is similar in both Ni and Ti atoms. In particular, (111), (112), (131) and (132) are the sites where Ni and Ti prefer to bind more strongly. Among these sites, 132 and 131 are the most favorable ones with a binding of -3.17 and -3.67 eV for Ni and -6.12 and -7.98 eV for Ti, respectively. It should also be noted that Ti binds to oxidized SWNT stronger than Ni: e.g., for (131) its binding is lower in energy compared to that of Ni by 4.31 eV. Based on these results, (111) and (131) site has been used in the hydrogen adsorption screening study.

Our results in far sites from carboxylic group show that Ti preferably positioned on hexagonal hollow sites instead of bridge sites while binding energy ranging from -2.5 eV to -3.1 eV, consistent with Yildirim et al.'s -2.2 eV [52], Durgun et al.'s -2.9 eV [70] and Sun et al.'s -2.35 eV [71]. Our results regarding Ni decoration on far sites from carboxylic group are in agreement in terms of the most favorable binding site of Ni on SWNT and not in agreement in terms of binding energies with Yang et al.'s results [72]. Binding energy of Ni on defect-free side of nanotube is 1.5 eV lower than Yang et al. This outcome could be attributed to higher curvature effect since we have smaller diameter SWNT. Furthermore, we observed that Ni binding was

enhanced about ~ -2.5 eV in close sites of $-OOH$, e.g. (111), (112), (131) and (132) with respect to results of Yang et al. [72].

Table 5.2 : Adsorption energies of Ni and Ti metals on 13 different adsorption sites of the oxidized SWNT

Adsorption sites (see Fig. 5.4)	Ni [eV]	Ti [eV]
(111)	-3,34	-5,39
(112)	-3,03	-5,72
(113)	-1,89	-2,78
(114)	-1,93	-2,86
(115)	-2,02	-2,75
(121)	-1,92	-3,05
(122)	-2,03	-2,56
(123)	-2,01	-2,73
(131)	-3,67	-7,98
(132)	-3,17	-6,12
(133)	-1,91	-2,84
(134)	-1,94	-2,83
(135)	-1,91	-2,88

5.3.2. Hydrogen adsorption on Ni and Ti doped, oxidized SWNTs

To adsorb hydrogen on Ni and Ti doped oxidized SWNT's, in addition to the most favorable metal sites, 111 and 131, other two sites, 135 and 115, were also considered for a better comparison. Since metal atoms are in interaction with $-OOH$ group in 111 and 131 orientations, binding of hydrogen might be higher in energy compared to the 135 and 115 sites where metal atoms are further away from the $-OOH$ group. The calculated binding energy of hydrogen in Ni and Ti doped 11, 131, 135 and 115 sites were listed in Table 5.3 and the optimized geometries were shown in Fig. 5.7.

For both metals, the binding energies were obtained much higher than the non-doped SWNT's mentioned in section 5.2.2. Only for Ti(131), a very low binding, $-0,07$ eV, was calculated, which merely achieved 0.24 wt.% hydrogen uptake. This means that within the presence of $-OOH$, only one Ti metal occupation cannot reach the desired hydrogen uptake of 9 wt.%[1] as Sun et al. expressed [71]. As seen from the Table 5.2, hydrogen binding energies increase on the (131) and (135) sites, where metal

atoms are in interaction only with the tube and hydrogen. In particular, for Ni(115) , Ni(135), Ti(115) and Ti(135), the calculated hydrogen binding energies were -1.00 eV, -0,99 eV, -0,83 eV and -1,00 eV, respectively. All these values show that binding of hydrogen in these sites are too strong.

Hydrogen favors the metal atoms which are far away from the carboxylic acid group, since *d* orbital vacancies of Ti and Ni [52, 73, 74], 8 and 2, respectively, are used when the metal atoms are in interaction with the carboxylic acid group (111 and 131 sites). It is known that *d* orbitals in titanium are more delocalized [50] and therefore the unfilled *d* orbitals of titanium may be hybridized with *2p* orbitals of the carboxylic acid group. As a result, hydrogen binds very weak to Ti(131) site compared to Ni(131). It is apparent from the Table 5.3 that hydrogen binds much stronger in Ni doped SWNT's compared to Ti ones. Moreover, the hydrogen binding energy obtained for Ti(115) is in excellent agreement with Yildirim et al.[52].

Table 5.3 : Adsorption energies of hydrogen on Ni and Ti doped (111), (115), (131) and (135) sites of oxidized SWNT

Adsorption sites (see Fig. 5.4)	Hydrogen Adsorption Energies [eV]	
	Ni-O-SWNT*	Ti-O-SWNT**
(111)	-0,54	-0,36
(115)	-0,99	-0,83
(131)	-0,45	-0,07
(135)	-0,99	-1,00

*Ni-O-SWNT: Ni doped, oxidized SWNT.

**Ti-O-SWNT: Ti doped, oxidized SWNT.

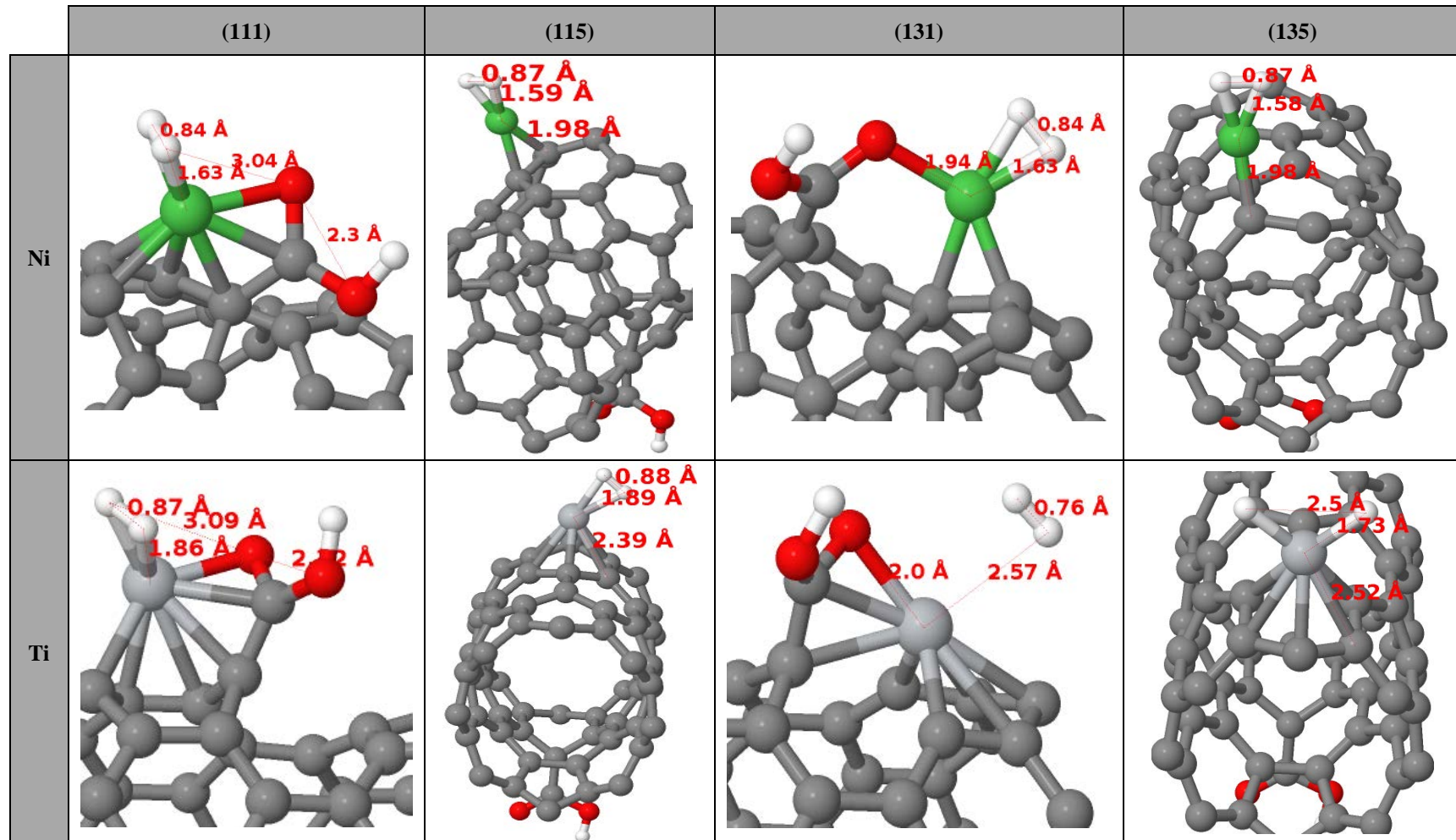


Figure 5.7 : Hydrogen adsorption on Ni, Ti doped (111), (115), (131) and (135) sites

5.3.3. Metal doped oxidized SWNT's

Calculations performed for Ni and Ti doped oxidized SWNT's showed that the best binding site for the metal atom is either 131 or 111. Therefore, these sites have been used to study the adsorption of the other metal species shown in Fig. 5.6 including Ca(194 pm), Co(152 pm), Cr(166 pm), Fe(156 pm), Mn(161 pm), Pd(169 pm), Pt(177 pm), Rh(173 pm), Ru(178 pm), Sc(184 pm), V(171 pm) and Y(212 pm). In the parenthesis, the calculated atomic radius of metals is given.

To calculate binding energy of the metal atoms, likewise for Ni and Ti, metal atoms have been placed into a cubic cell with a cell parameter, $a = 10 \text{ \AA}$ and $(8 \times 8 \times 8)$ k -points have been employed. Binding energy results corresponding to local min states of 12 metals are given in Table 5.4.

Table 5.4 : Binding site of single adatom on (111) and (131) of (8,0) oxidized SWNT (H :hexagonal site, B :bridge site of C-C bond, V :into the vacancy), min carbon-adatom bond distance (d_{m-c}), min dangling oxygen-adatom bond distance (d_{m-o}), calculated binding energies of individual adatoms occupied on (111) and (131) of (8,0) oxidized SWNT (E_{ads}).

Metals	(111)				(131)			
	Site	d_{m-c} [Å]	d_{m-o} [Å]	E_{ads} [eV]	Site	d_{m-c} [Å]	d_{m-o} [Å]	E_{ads} [eV]
Ca	H	2,55	2,16	-3,55	H	2,54	2,26	-3,82
Co	B-H	2,1	2,02	N.A.	B-V	1,83	2,06	N.A.
Cr	B-H	1,99	2,01	-5,77	B-V	1,86	1,91	-8,16
Fe	B-H	1,98	2,08	-5,26	B-V	1,83	2,01	-7,49
Mn	B-H	1,96	2,05	-5,59	B-V	1,84	1,99	-7,82
Pd	H	2,12	3,34	-1,60	B	2,14	2,31	-1,95
Pt	H	2,09	3,38	-2,84	B	2,09	2,24	-3,11
Rh	B-H	2,09	2,35	-3,91	B-V	1,94	2,06	-6,45
Ru	B-H	2,29	2,15	-5,01	B-V	1,97	2,47	-7,45
Sc	B-H	2,02	2,27	-5,03	B	2,17	2,06	-5,57
V	B-H	1,97	2,02	-5,65	B-V	1,88	1,93	-8,23
Y	B-H	2,4	2,15	-5,11	B	2,31	2,21	-5,61

As indicated in Table 5.4, the resulting binding energies are in between -0.2 and -8.0 eV. Thus, all considered metal atoms prefer to bind to the oxidized SWNT. Except Ca, Co, Ni, Pd and Pt, for the remaining metals binding to (131) site is more favorable. For Ca, Co, Ni, Pd and Pt, binding energies were calculated to be similar in both (111) and (131) sites. Except of Ca, Ni, Pd, Pt, Rh, all of selected metals were occupied with binding energy range of 5.0-5.8 eV. Among the considered metals the

least tendency to the oxidized SWNT was found for Co. The strongest binding (around -8 eV) to the SWNT was obtained for V, Cr, Ti and Mn. Honestly we can say that calculations results are consistent with Durgun et al.'s study [70] and Wu and Zeng's study [75] in the context of occupation location of metals on SWNT. However, it is so obvious that carboxylic group has strongly enhanced binding energies of occupied metals (except of Pd and Pt) from the range of -2.0 and -3.7 eV to the range of -3.6 and -8.0 eV in comparison with Durgun et al.'s [70] and Wu-Zeng's [75]. Even there is no a direct relation between the atomic radius of metals and the binding energy, metals with higher atomic radius tend to be placed into the vacancies or onto the hexagons. In the next section, one hydrogen molecule will be added to these metals doped oxidized SWNT's to determine the most effective metal species.

5.3.4. Hydrogen adsorption on metal doped oxidized SWNT's

A hydrogen molecule was added to the geometries obtained at the previous section to investigate the binding energy of hydrogen onto the metal doped oxidized SWNT's. Since the most favorable metal sites are (111) and (131), only these two sites used in the screening and hydrogen molecule was placed approximately 2 Å away from the carboxylic acid group and then the whole system was relaxed. The resulting binding energies were shown in Fig. 5.8. Moreover, the final geometries for (111) and (131) sites were included in Figs. 5.9 and 5.10, respectively

As clear from the Fig 5.9, hydrogen prefers (111) site rather than (131) site. For (111) site, except Ca, Ni, Pd, Pt, Sc, Ti and Y, hydrogen binding was calculated to be around zero, indicating that there is no practical binding. Moreover, the binding energy of hydrogen on Ca, Ti and Y was approximately -0.1 eV. In Fig. 5.8, the best hydrogen binding region between -0.20 and -0.60 eV was shown in yellow. For the (111) site, only Ni, Pd and Pt located in this best region. In contrast to (111), (131) site leads to much higher hydrogen binding energies. Except Mn, Ca, Sc, Ti, V and Y, hydrogen binding energies were matched to the best binding region.

The resulting geometries shown in Figs. 5.9 and 5.10 were similar to each other except Ca, Pd and Pt where the metal atoms were not positioned towards the bridge site of axial C-C bond and oxygen of the carboxylic group. In particular, Ca was

relocated relatively far from C-C bridge site which is close to the single oxygen. Pd and Pt were placed at the centre of (111) site and approximately 3.3 Å away from one of the oxygen of the carboxylic group. This value is almost 1.3 Å greater than that of the other metal species. Furthermore, the distance between hydrogens were found between 0.76 – 0.93 Å.

At the (131) site, metal positions in the relaxed structures were not similar to each other in contrast to (111) site. More specifically, Ca was placed 2.54 Å away from the nearest carbon and 2.26 Å from one of the oxygen and the hydrogen molecule was positioned 2.8 Å away from Ca. Furthermore, we noticed that Ca binding energies on sites was enhanced within the presence of –OOH group as already shown by Lee et al. [79]. In particular, Ca binding energies with -3.55 eV and -3.82 eV for (111) and (131) positions, respectively, are in quite agreement with the findings of Lee et al. [76], which is -3.30 eV. Since it has already been proven that the binding energy of hydrogen onto transition metals increases via the hybridization of the *d* levels with the H₂ states [47], the weak of hydrogen binding energies in (111) and (131) sites could be only attributed to the depletion of charge transfer from Ca-C to Ca-H₂ by –OOH group.

Although Pd and Pt have been occupied on (131) with similar binding distances from the nearest carbon by 2.1 Å and dangling oxygen by 2.31 Å, 2.24 Å respectively, binding energy of adsorbed hydrogen molecule is almost two times lower in energy at Pt(131) than Pd(131). A similar situation was also observed for Pt(111) and Pd(111). Moreover, Pt binding energies with -2.84 eV and -3.11 eV for (111) and (131) positions, respectively, are close to the findings of Park et al. [16] to be -2.45 eV obtained for the bridge site of defect-free (8,0) SWNT, -3.28 eV obtained for the stone-wales defected of (8,0) SWNT and -6.40 eV obtained in the mono-vacancy of (8,0) SWNT. When compared with the binding energy between Pt and SWNT found by Dag et al., -2.92 eV, for the single Pt doped pure (8,0) SWNT, oxidization reduces this value to -2.84 eV and -3.11 eV for (111) and (131) positions, respectively. This strong binding between Pt and oxidized SWNT weakens the hydrogen binding to -0.57 eV and -0.51 eV for (111) and (131) positions, respectively. This could be attributed to the strengthened Pt-O binding which ultimately leads to less charge transfer to Pt-H.

Among the rests except of Sc and Y, tended to move into the octahedral arrangement by splitting over C-C bond indicated with orange of pentagonal ring. The smallest distance in the bond formed by the combination of the dangling bonds on the pentagonal ring (See Fig. 5.2) was obtained for Co to be 2.51 Å and this distance was maximum for V to be 2.69 Å.

As indicated in the previous sections, if hydrogen is placed on sites such as (115) or (135), hydrogen binds very strongly, approximately -1.0 eV. However, this value is beyond the maximum limit which is almost -0.6 eV.

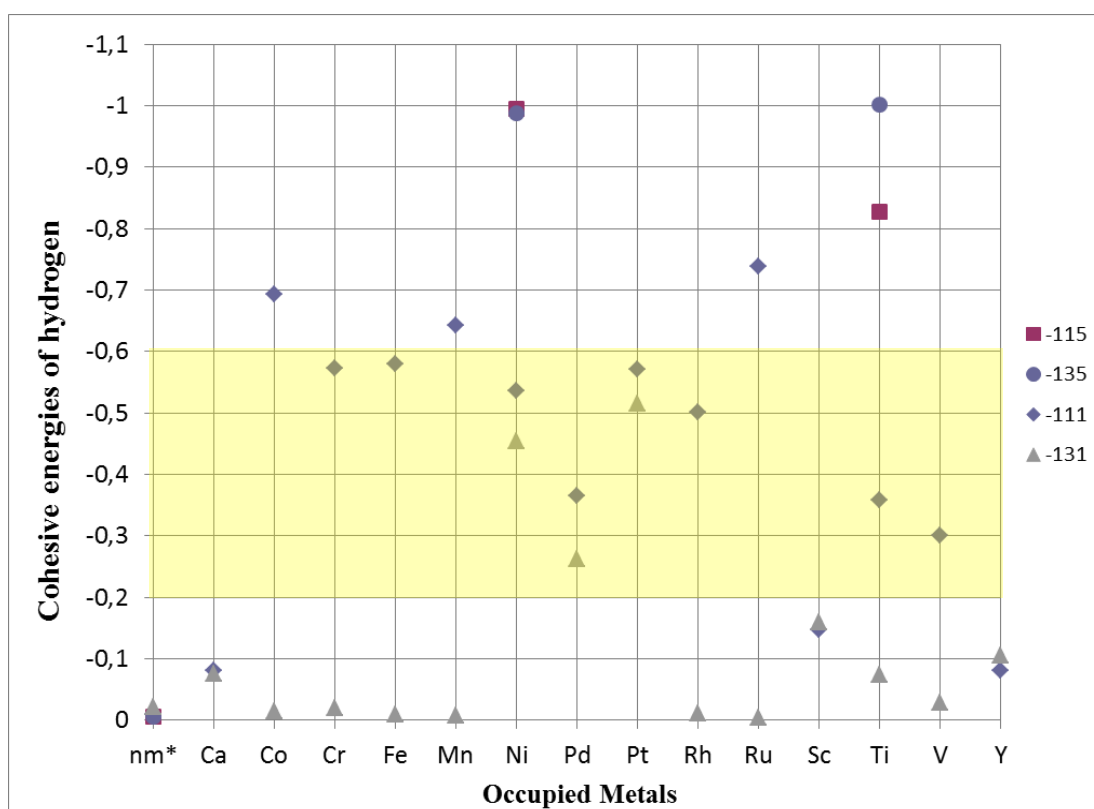


Figure 5.8 : Hydrogen binding energies [eV] onto the metal doped oxidized SWNT's

*nm: the case of hydrogen adsorption without metal

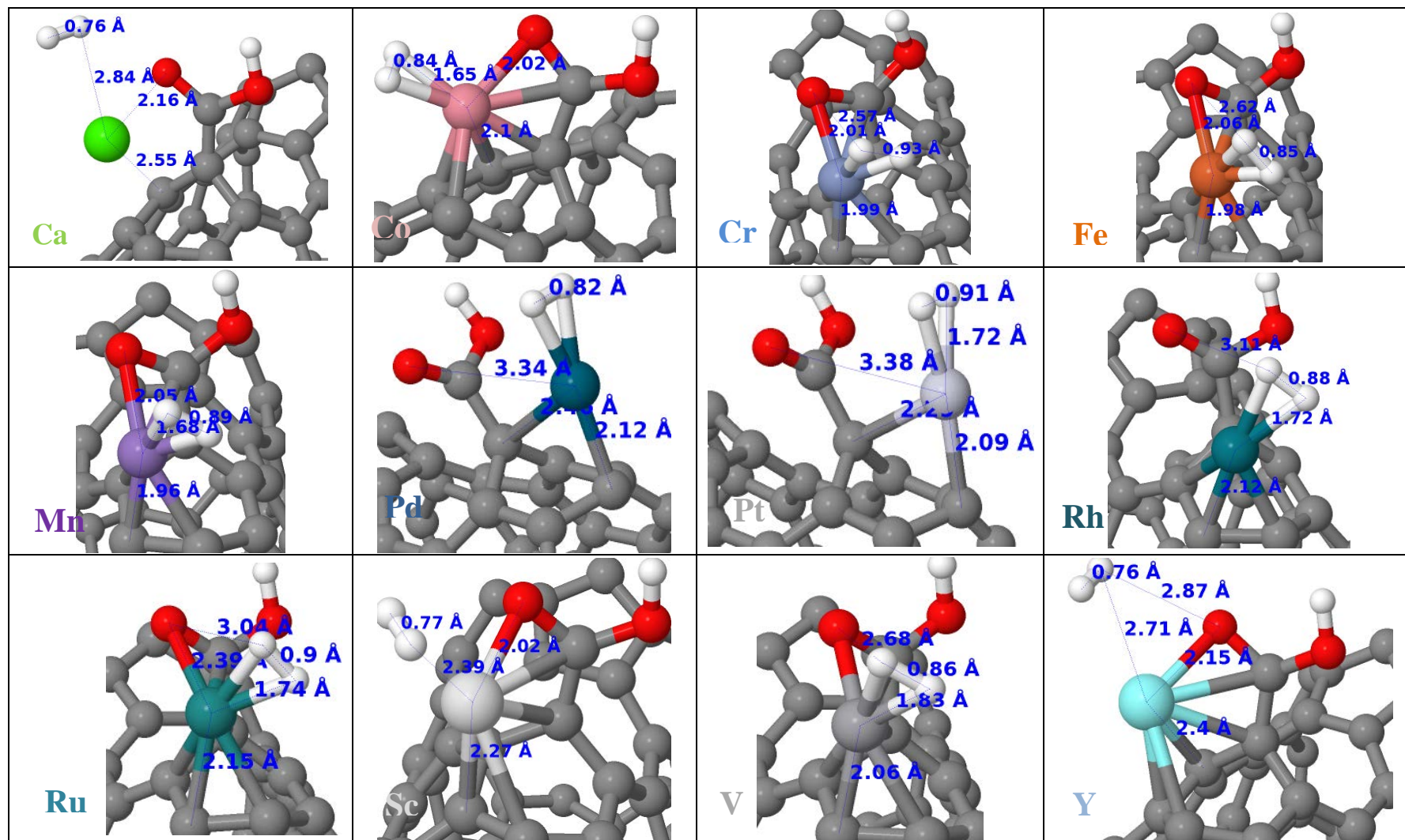


Figure 5.9 : Hydrogen adsorbed geometries of (111) metal doped oxidized SWNT's.

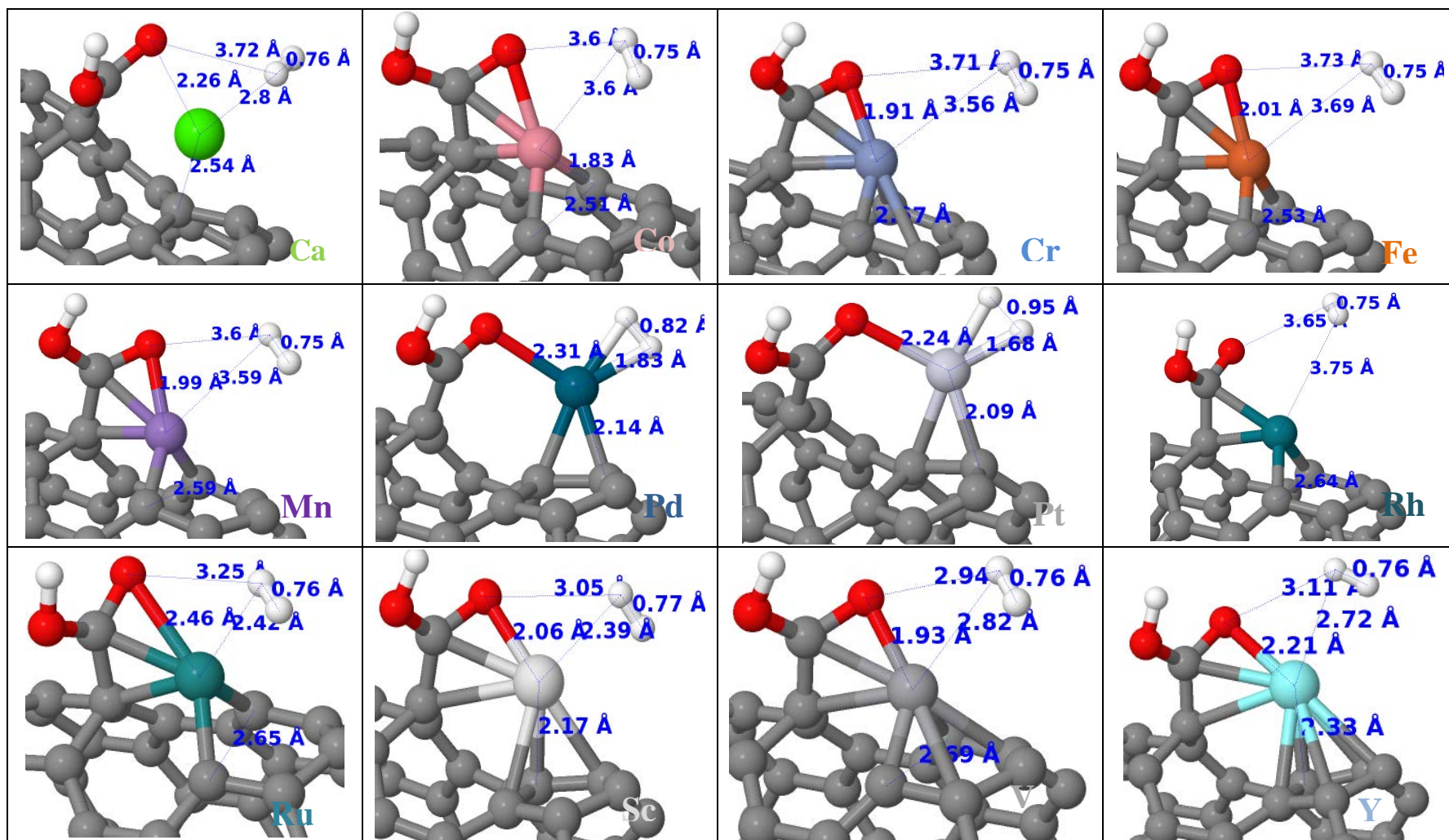


Figure 5.10 : Hydrogen adsorbed geometries of (131) metal doped oxidized SWNT's.

5.3.5. Clustering of metals

Up to now, only one metal atom was considered in this screening study. However, some of the metal atoms may prefer clustering rather than staying as individual atoms. To investigate this phenomenon, 4 metal atoms have been placed as individuals, onto of carboxylic group and further away from the carboxylic group. These three different binding sites allow determining whether the metal atoms do clustering and if so whether they do it on the carboxylic group or not. Besides 4 metal atoms, several bigger systems were also investigated but not for all metal species. Recently, Sun et al. [71] showed that Ti atoms prefer clustering around the carbon buckyball. Therefore, they claimed that amount of absorbed hydrogen onto the SWNT is reduced due to the clustering. Only Ti atoms positioned at outermost shell are able to absorb hydrogen, however, the ones in the inner shell are not capable of binding the hydrogen. This fact reduces the amount of absorbed hydrogen, nearly 7.5 wt %, to considerably low values, 2.85 wt % [71]. Currently, only Ca, Fe, Ni, Pd, Pt and Ti metals have been considered to investigate the clustering phenomenon. As described above, three possible clustering positions were examined: (i) clustering above the carboxylic group, (ii) clustering on the plane side of oxidized SWNT (opposite side of $-OOH$ group, abbreviated as R-OOH) and (iii) distribution through circumferential axis. Four metals were positioned as lozengelike for these three cases. Above the $-OOH$ group, one of 4 metals was initially located on the front side of $-OOH$ and the other one on back side; in other words on (131) and (111) sites, respectively. Lateral atoms were located adjacent sites to $-OOH$ group. For the second case, similar with first case two of them were placed axially on (135) and (115), respectively; the rests on zigzag adjacent sites such as (123) and symmetry of (123) with respect to axial distributed atoms. For the third case, each of four metals was initially placed on hexagonal sites as lozengelike on the circumferential axis. All the resulting geometries are shown in Fig. 5.11 and all the corresponding binding energies are listed in Table 5.5.

Coherently with single Ca atom decoration (see Fig. 5.9-10), 4 Ca atoms replaced after relaxation in far positions from hexagonal spaces with binding distance range of $2.47 \text{ \AA} - 2.78 \text{ \AA}$ to the nearest carbon; instead of forming cluster. In circumferential

distribution, binding energies per Ca atom on hexagonal spaces with -1.62 eV is consistent with the results of Lee et al.'s boron doped and Ca doped fullerene [76].

Table5.5 : Binding energies [in eV] of the oxidized SWNT's doped by four metal atoms at -OOH, R-OH and circumferential sites.

Metal Species	-OOH site	R-OOH site	Circumferential site
Ca	-1,98	-1,31	-1,62
Fe	-4,71	-4,52	-3,86
Ni	-3,11	-2,87	-2,37
Pd	-1,69	-1,72	-1,35
Pt	-3,13	N.A	N.A.
Ti	-5,69	-4,30	-3,83

In the case of Ca, similar to single Ca decoration (see Fig. 5.9-10), 4 Ca atoms relaxed far away from the hexagonal spaces with a binding distance range of 2.47 – 2.78 Å to the nearest carbon. Clearly, Ca does not prefer clustering. In circumferential decoration, binding energies per Ca atom on hexagonal spaces obtained to be -1.62 eV and this value is close to the results of Lee et al. found for boron doped and Ca doped fullerene [76].

As seen from the Fig 5.11, Pd atoms do clustering. However, they prefer R-OOH site rather than -OOH site. The corresponding binding energy per Pd atom was calculated to be -1.69 eV, -1.72 eV and -1.35 eV for three cases, respectively. A similar situation was observed for Fe. Inclusion of more Pd and Fe atoms may result a clustering at the above of -OOH like Ni and Ti.

Pt clustering on first case has significant outcomes in comparison with the results of Dag et al.[47]. Contrary to the popular concept [47], although binding energies of Pt was supposed to increase with the increased number of Pt atoms from 1 to 4 atoms, binding energies of Pt was not increased, instead, they remained around -3.11 eV. Middle Pt atom of the cluster above the-OOH group prefers to bind on the centre of hexagonal site (Fig. 5.12) similar to the case Pt(111) shown in Fig. 5.9. Moreover, it can be noticed that neighbouring carbon atom in the hexagonal ring, across the middle Pt, was titled by Pt cluster with 2.4 Å binding distance to middle Pt and single Pt atom on (131) site was relocated on C-C bridge site with similar binding distances as in Pt(131) shown in Fig. 5.10.

Calculations carried out with 4 Ti atoms in 3 different cases show that Ti atoms do clustering above the –OOH group with relatively higher binding energies to be 1.39 eV/Ti and 1.85 eV/Ti higher than the R–OOH and circumferential positions, respectively. These results are in consistent with Sun et al. [71] and indicates that high amount of absorbed hydrogen onto the circumferential positions is not realistic. [52]. On the other hand, similar to Pt cluster on –OOH group, 3 Ti prefer to bind triangularly while the middle one relocated on the pentagon and two adjacent Ti atoms on C-C bridges.

Only for Ti, a specific set of cluster calculations were carried out with 6, 9 and 11 Ti atoms on –OOH group. Although metal binding energy was increased to 6.17 eV/Ti for 6 Ti, in later calculations reduced to 5.54 eV/Ti and 5.46 eV/Ti for 9 and 11 Ti, respectively.

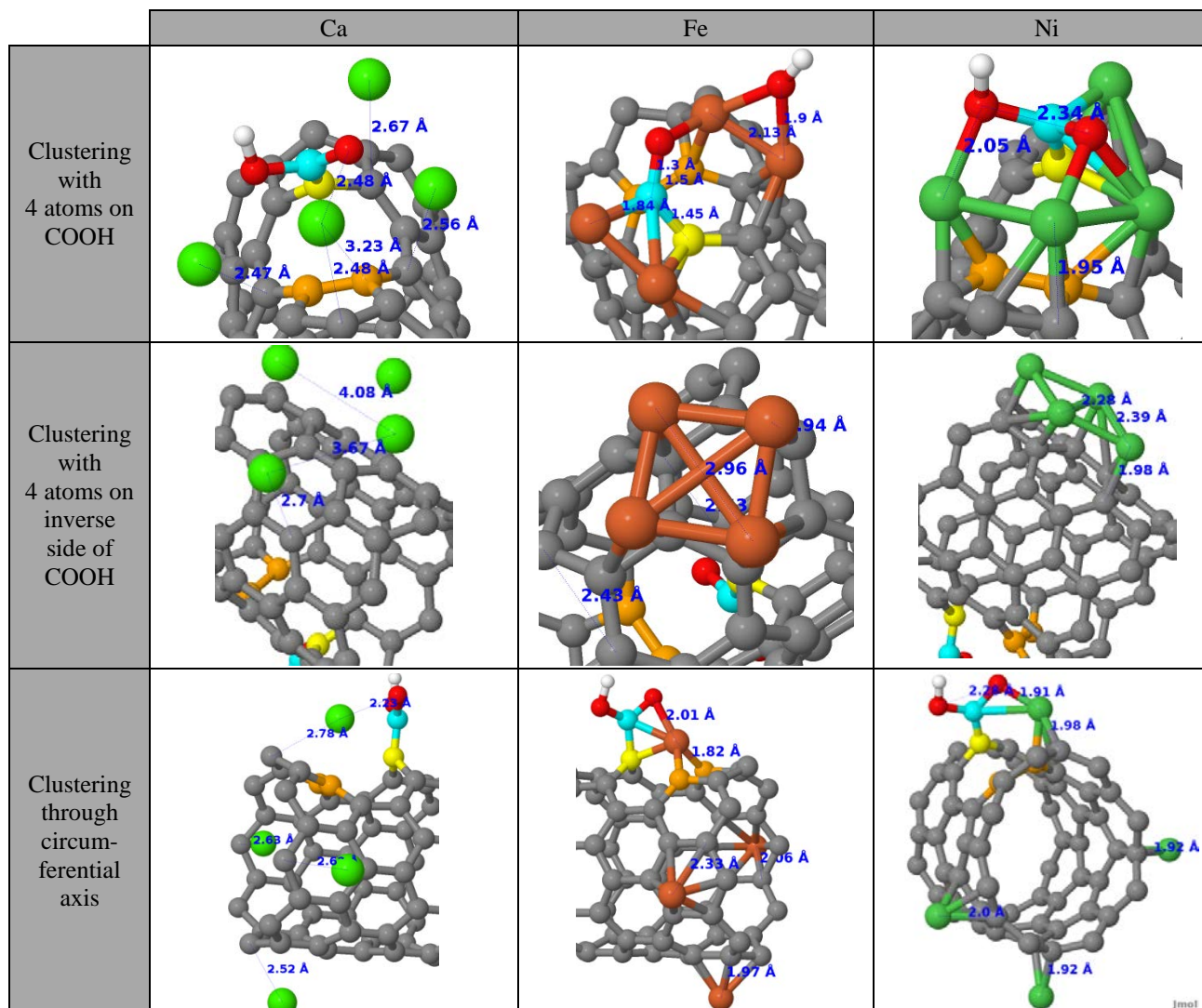


Figure 5.11 : Optimized geometries of Ca, Fe and Ni clustered oxidized SWNT

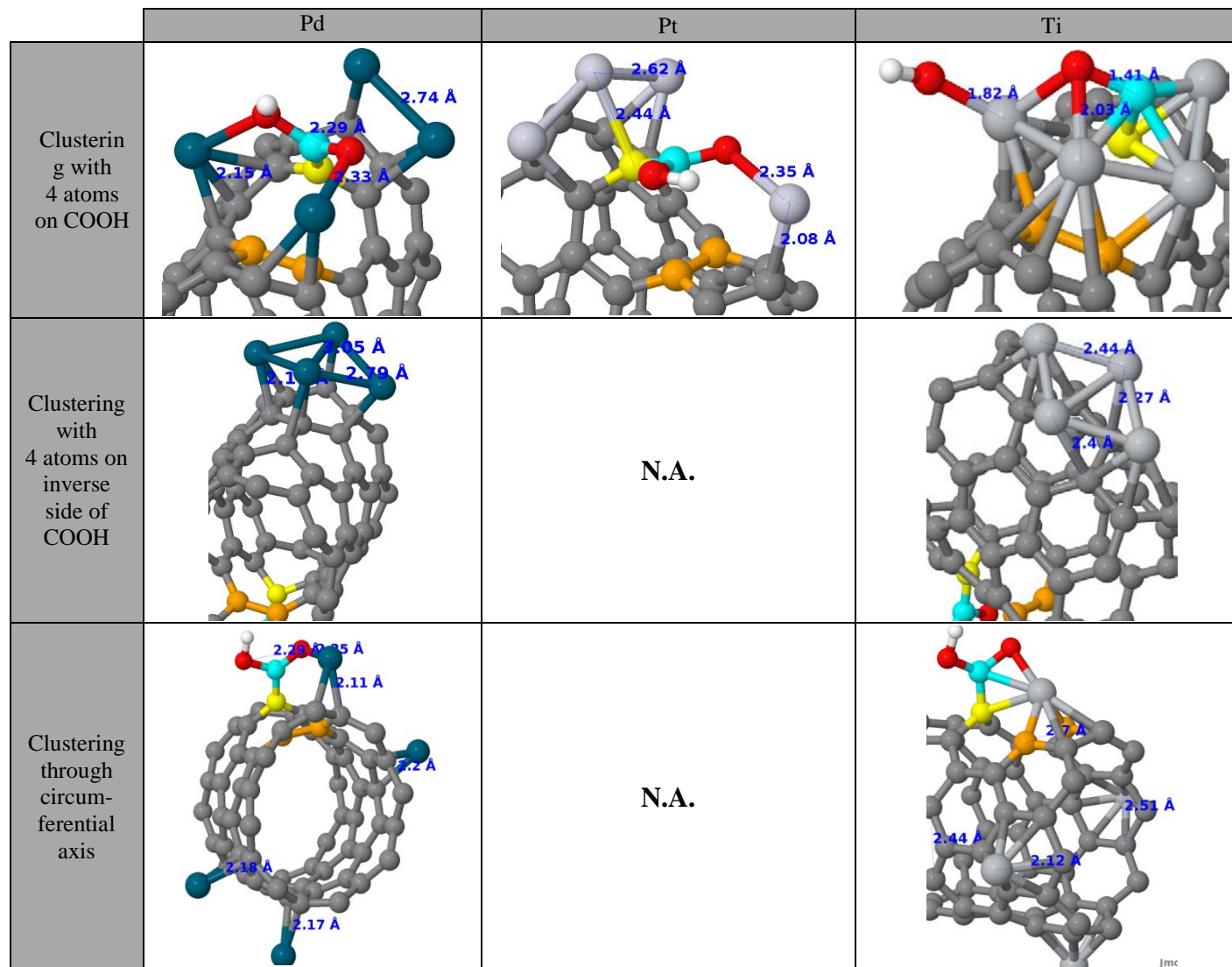


Figure 5.12 : Optimized geometries of Pd, Pt and Ti clustered oxidized SWNT

6. SUMMARY, CONCLUSIONS AND FUTURE WORK

Hydrogen has been recognized as a highly appealing energy carrier for renewable energy applications as well as owning of arduous storage conditions. The carbon nanotubes have been widely studied for hydrogen storage applications [1,2] due to having high storage capacities by structural modifications, e.g. defects, oxidized groups, vacancies, metal decoration on CNT [3-17]. In this study, we tried to understand the effect of vacancy creation, effect of oxidative functionalization, effect of metal decoration in presence of carboxylic group and hydrogen adsorption in these conditions on SWNT. For this purpose, a screening study employing periodic DFT was performed using Ca, Co, Cr, Fe, Mn, Ni, Pd, Pt, Rh, Ru, Sc, Ti, V and Y metal species.

In the first step of the computational study, an atomic vacancy was created on the sidewall of SWNT and carboxylic functionalization was carried out on this vacancy. Corresponding to three related structures: pristine, with vacancy and oxidized SWNT; electronic property of nanotube was permanently changed from semi-conductor to metallic. Beside this, it has been found that hydrogen does not bind to the SWNT in the vicinity of $-OOH$ group.

In the case of metal doped oxidized SWNT, it has been observed that close sites to $-OOH$ group were more favorable for metal decoration. Therefore, hydrogen molecules were added to these systems to determine how strongly hydrogen can bind to metal doped oxidized SWNT. The best hydrogen adsorption values were calculated for the following metals: Ni, Pd and Pt, in the range of -0.2 and -0.6 eV. Contrary to the early findings indicating that transition metals such as Ti and V have the best hydrogen binding capacities in metal decorating calculations, situation completely changes when metals doped close to $-OOH$ group. Furthermore, metal decoration with Ca, Sc, Y, Ti and V do not lead to high hydrogen binding energies. This evaluation could be attributed to how much d orbital hybridization of metals with carbons and hydrogens enhances the binding. To investigate whether metals do clustering or not, 4 metal

atoms were positioned onto the oxidized SWNT in a 3 different ways: (i) clustering above the carboxylic group, (ii) clustering on the opposite site of –OOH group and (iii) distribution through the circumferential axis. Clustering is only studied for Ca, Fe, Ni, Pd, Pt and Ti. Clustering calculations showed that Ca, Fe, Ni and Ti tend to form clusters onto the carboxylic group and only Pd prefers a clustering at the plane side of SWNT. Distribution through the circumferential axis was not preferable in any case. These results show that amount of absorbed hydrogen cannot reach to the values appeared in the literature such as 7.5 wt. %. Instead, maximum storage dramatically reduces to nearly 3.0 wt. %.

Our results advance our fundamental understanding of metal decoration in presence of carboxylic group, hydrogen adsorption in metal doped oxidized SWNT and suggest new routes to better storage systems. Obviously, investigating the effect of different parameters in our calculations is an immediate further work that can easily be performed. In the first instance, hydrogen binding capacities of metal cluster structures would be explored in a bigger unit cell. Furthermore, in order to examine the structural effects, functional group(s) could be replaced in different sites. We hope that these computational studies motivate an active line of experimental efforts towards novel materials needed for hydrogen storage.

REFERENCES

- [1] **Ströbel R., Garche J., Moseley P. T., Jörissen L., Wolf G.,**(2006).Hydrogen Storage by Carbon Materials, *Journal of Power Sources*, **159**,781-801
- [2] **Bénard P.andChahine R.,** (2007). Storage of Hydrogen By Physisorption On Carbon And Nanostructured Materials, *ScriptaMaterialia*, **56**, 803–808
- [3] **Lee S.Y. and ParkS. J.,** (2010).Effect of Temperature on Activated Carbon Nanotubes for Hydrogen Storage Behaviors, *International Journal of Hydrogen Energy*,**35**, 6757- 62
- [4] **Wu H., Wexler D., Ranjbartoreh A.R., LiuH., Wang G.,** (2010).Chemical Processing of Double-Walled Carbon Nanotubes for Enhanced Hydrogen Storage, *International Journal of Hydrogen Energy*,**35**, 6345-49.
- [5] **Chen X.,Zhang Y.,Gao X. P.,Pan G. L.,Jiang X. Y.,Qu J. Q.,Wu F.,Yan J., Song D. Y.,**(2004).Electrochemical Hydrogen Storage of Carbon Nanotubes and Carbon Nanofibers, *International Journal of Hydrogen Energy*,**29**, 743-48.
- [6] **Cheng H. M., Yang Q. H., Liu C.,** (2001).Hydrogen Storage in Carbon Nanotubes, *Carbon*,**39**, 1447–54.
- [7] **Tibbetts G. G., Meisner G. P., Olk C. H.,** (2001). Hydrogen Storage Capacity of Carbon Nanotubes, Filaments and Vapor-Grown Fibers, *Carbon*,**39**, 2291-2301.
- [8] **Li X., Zhu H., Xu C., Mao Z., Wu D.,** (2003).Measuring Hydrogen Storage Capacity of Carbon Nanotubes by Tangent-Mass Method, *International Journal of Hydrogen Energy*,(28), 1251-53.
- [9] **Luxembourg D., Flamant G., Beche E., Sans J. L., Giral J., Goetz V.,** (2007). Hydrogen Storage Capacity at High Pressure of Rawand Purified Single-Walled Carbon Nanotubes Produced With A Solar Reactor, *International Journal of Hydrogen Energy*,**32**, 1016-23.
- [10] **Pan W., Zhang X., Li S., Wu D., Mao Z.,** (2005).Measuring Hydrogen Storage Capacity of Carbon Nanotubes by High-Pressure Microbalance, *International Journal of Hydrogen Energy*,**30**, 719-22.
- [11] **Ioannatos G. E. andVerykios X. E.,** (2010).H₂Storage on Single- and Multi-Walled Carbon Nanotubes, *International Journal of Hydrogen Energy*,**35**, 622-28.

- [12] **Ni M., Huang L., Guo L., Zeng Z.**, (2010).Hydrogen Storage in Li-Doped Charged Single-Walled Carbon Nanotubes, *International Journal of Hydrogen Energy*,**35**, 3546-49
- [13] **Park S. J. and Lee S. Y.**, (2010).Hydrogen Storage Behaviors of Platinum-Supported Multi-Walled Carbon Nanotubes, *International Journal of Hydrogen Energy*,**35**, 13048-54
- [14] **Surya V. J.,Iyakutti K.,Venkataramanan N.,Mizuseki H.,Kawazoe Y.**,(2010).The Role of Li and Ni Metals in The Adsorbate Complex and Their Effect on The Hydrogen Storage Capacity of Single Walled Carbon Nanotubes Coated With Metal Hydrides, LiH And NiH₂, *International Journal of Hydrogen Energy*,**35**, 2368-76
- [15] **Chen Y.,Wang P.,Liu C.,Cheng H. M.**, (2007).Improved Hydrogen Storage Performance of Li–Mg–N–H Materials by Optimizing Composition and Adding Single-Walled Carbon Nanotubes, *International Journal of Hydrogen Energy*,**32**, 1262-68
- [16] **Park Y.,Kim G., Lee Y. H.**,(2008). Adsorption and Dissociation of Hydrogen Molecules on A PtAtom on Defective Carbon Nanotubes, *Applied Physics Letter*, **92**, 66-70
- [17] **Gayathri V.andGeetha R.**, (2007). Hydrogen Adsorption in Defected Carbon Nanotubes, *Adsorption*, **13**, 53-59
- [18] **Hou P., Liu C., Cheng H.**, (2008). Purification of Carbon Nanotubes, *Carbon*, **46**, 2003-25
- [19] **DOE Hydrogen Program**, (2009). Fuel Cells for Backup Power in Telecommunications Facilities [online]. Retrieved February 21, 2012 from <http://www.hydrogen.energy.gov/pdfs/44520.pdf>
- [20] **Atay G.**, (2005). An Investigation of Hydrogen Storage in Carbon Nanotubes via Computational Mm Methods. Master of Science Thesis, Boğaziçi University Chemical Engineering, Istanbul, Turkey.
- [21] **Züttel A.**,(2008). Hydrogen Report Switzerland. Retrieved February 22, 2012 from http://www.empa.ch/plugin/template/empa/*/73305
- [22] **Hirscher M.**,(2010). *Handbook of Hydrogen Storage: New Materials for Future Energy Storage*. Published by WILEY – VCH Verlag GmbH & Co. KGaA, Weinheim, Germany
- [23] **Çimen T.**,(2006). SıvıHidrojenTanklarınınIsılAnalizive Optimal Tasarımı. Master of Science Thesis, Istanbul Technical University Institute of Energy, Istanbul, Turkey.
- [24] **Wu Y. andMohring R. M.**,(2003). Sodium Borohydride For Hydrogen Storage, *American Chemical Society, Division of Fuel Chemistry*, **48**(2), 940

- [25] **Rowell J. L. C., Yaghi O. M.,**(2005). Strategies for Hydrogen Storage in Metal–Organic Frameworks, *Angewandte Chemie International Edition*, **44**, 4670-79
- [26] **Murray L. J., Dinca M., Long J. R.,** (2009). Hydrogen Storage in Metal–Organic Frameworks, *RSC Chemical Society Reviews*, **38**, 1294-1314
- [27] **Bénard P. and Chahine R.,** (2001). Modeling of Adsorption Storage of Hydrogen on Activated Carbons, *International Journal of Hydrogen Energy*, **26**, 849–55
- [28] **Zhao W., Fierro V., Zlotea C., Aylon E., Izquierdo M. T., Latroche M., Celzard A.,**(2011). Optimization of Activated Carbons for Hydrogen Storage, *International Journal of Hydrogen Energy*, **36**, 11746-51
- [29] **Iijima S.,**(1991). Helical Microtubules of Graphitic Carbon, *Nature*, **354**, 56–8.
- [30] **Iijima S. and Ichihashi T.,**(1993). Single-Shell Carbon Nanotubes of 1-Nm Diameter, *Nature*, **363**, 603–15
- [31] **Chen, Z.,** (2007). Single-Walled Carbon Nanotubes (SWNT) Polymer Composites & Composite Fibers. Phd Thesis, Rice University, Houston/Texas, USA.
- [32] **Saito R., Dresselhaus G., and Dresselhaus M.S.,** (1998). *Physical properties of carbon nanotubes*. Imperial College Press, London.
- [33] **Niyogi S., Hamon M. A., Hu H., Zhao B., Bhowmik P., Sen R., Itkis E., Haddon R. C.,**(2002). Chemistry of Single-Walled Carbon Nanotubes, *Accounts of Chemical Research*, **35**, 1105-13
- [34] **Dresselhaus M. S., Dresselhaus G., Charlier J. C., Hernandez E.,**(2004). Electronic, Thermal and Mechanical Properties of Carbon Nanotubes, *Philosophical Transactions of the Royal Society A*, **362**, 2065–98
- [35] **Charlier J.-C., Gonze X., Michenaud J.-P.,**(1991). First-Principles Study of The Electronic Properties of Graphite, *Physical Review B*, **43**, 4579-89.
- [36] **Loiseau A., Launois P., Petit P., Roche S., Salvétat J.-P.,**(2006). *Understanding Carbon Nanotubes from Basics to Applications*, Springer-Verlag, Berlin, Germany
- [37] **Andrews R.,** (2001). Carbon Nanotubes: Synthesis, Properties, and Applications, *Critical Review of Solid State Materials Science*; **26** (3), 145-249
- [38] **Hauke F. and Hirsch A.,**(2010). Covalent Functionalization of Carbon Nanotubes, *Carbon Nanotubes and Related Structures*, WILEY-VCH Verlag GMBH & Co. KGaA, Weinheim, Germany

- [39] **Tobias G., Shao L., Salzman C. G., Huh Y., Green M. L. H.,** (2006). Purification and Opening of Carbon Nanotubes Using Steam, *Journal of Physical Chemistry B*, **110**, 22318-22
- [40] **Wang C., Zhou G., Wu J., Gu B.-L., Duan W.,**(2006). Effects of Vacancy-Carboxyl Pair Functionalization on Electronic Properties of Carbon Nanotubes, *Applied Physics Letter*, **89**, 173130
- [41] **Zhao B., Hu H., Bekyarova E., Itkis M. E., Niyogi S., Haddon R. C.,**(2004). Carbon Nanotubes: Chemistry, *Dekker Encyclopedia of Nanoscience and Nanotechnology*, CRC Press, California, USA
- [42] **Herranz A. and Martín N.,**(2010). Noncovalent Functionalization of Carbon Nanotubes, Carbon Nanotubes and Related Structures, WILEY-VCH Verlag GMBH & Co. KGaA, Weinheim, Germany
- [43] **Gerber I., Oubenali M., Bacsá R., Durand J., Gonçalves A., Pereira M. F. R., Jolibois F., Perrin L., Poteau R., Serp P.,**(2011). Theoretical and Experimental Studies on the Carbon-Nanotube Surface Oxidation by Nitric Acid: Interplay between Functionalization and Vacancy Enlargement, *Chemistry – A European Journal*, **17**, 11467 – 77
- [44] **Kamaras K., Itkis M. E., Hu H., Zhao B., Haddon R. C.,**(2003). Covalent Bond Formation to a Carbon Nanotube Metal, *Science*, **301**, 1501
- [45] **Zhang J., Zou H., Qing Q., Yang Y., Li Q., Liu Z., Guo X., Du Z.,** (2003). Effect of Chemical Oxidation on the Structure of Single-Walled Carbon Nanotubes, *Journal of Physical Chemistry B*, **107**, 3712-18
- [46] **Wang C., Zhou G., Wu J., Gu B.-L., Duan W.,**(2006). Effects of Vacancy-Carboxyl Pair Functionalization on Electronic Properties of Carbon Nanotubes, *Applied Physics Letters*, **89**, 173130
- [47] **Dag S., Ozturk Y., Ciraci S., Yildirim T.,**(2005). Adsorption and Dissociation of Hydrogen Molecules on Bare and Functionalized Carbon Nanotubes, *Physical Review B*, **72**, 155404
- [48] **Itkis M. E., Niyogi S., Meng M. E., Hamon M. A., Hu H., Haddon R. C.,**(2002). Spectroscopic Study of the Fermi Level Electronic Structure of Single-Walled Carbon Nanotubes, *Nano Letters*, **2**(2), 155-9
- [49] **Volpe M. and Cleri F.,** (2003). Role of Surface Chemistry in Hydrogen Adsorption in Single-Walled Carbon Nanotubes, *Chemical Physics Letters*, **371**, 476–82
- [50] **Lee H., Ihm J., Cohen M. L., Louie S. G.,** (2009). Calcium-Doped Carbon Nanotubes for High-Capacity Hydrogen Storage: First-Principles Calculations, *Physical Review B*, **80**, 115412

- [51] **Bhattacharya S., Majumder C., Das G. P.,**(2008). Hydrogen Storage in Ti-Decorated BC₄N Nanotube, *The Journal of Physical Chemistry C*, **112**, 17487-91
- [52] **Yildirim T. and Ciraci S.,**(2005). Titanium-Decorated Carbon Nanotubes as A Potential High-Capacity Hydrogen Storage Medium, *Physical Review Letters*, **94**, 175501
- [53] **Shevlin S. A. and Guo Z. X.,**(2008). High-Capacity Room-Temperature Hydrogen Storage in Carbon Nanotubes via Defect-Modulated Titanium Doping, *The Journal of Physical Chemistry C*, **112**, 17456–64
- [54] **Bénard P., Chahine R., Chandonia P. A., Cossement D., Dorval-Douville G., Lafi L., Lachance P., Paggiaro R., Poirier E.,** (2007). Comparison of hydrogen adsorption on nanoporous materials, *Journal of Alloys and Compounds*, **446**, 380–4
- [55] **Wu H., Wexler D., Liu H.,**(2011). Effect of Different Reductants for Palladium Loading on Hydrogen Storage Capacity of Double-Walled Carbon Nanotubes, *International Journal of Hydrogen Energy*, **36**, 9032-36
- [56] **Bénard P. and Chahine R.,**(2007). Storage of hydrogen by physisorption on carbon and nanostructured materials, *Scripta Materialia*, **56**, 803-8
- [57] **Young D. C.,**(2001). Molecular Dynamics and Monte Carlo Simulations, *Computational Chemistry - A Practical Guide for Applying Techniques To Real-World Problems*, John Wiley & Sons, Inc., NY, USA
- [58] **Sholl D. S. and Steckel J. A.,**(2009). *Density Functional Theory – A Practical Introduction*, John Wiley & Sons, Inc., Hoboken, New Jersey, USA
- [59] **Moses P. G.,**(2008). Transition Metal Sulfide Catalysts — A DFT Study of Structure and Reactivity, Ph.D. Thesis, Technical University of Denmark, KongensLyngby, Denmark
- [60] **Koch W. and Holthausen M. C.,**(2001). *A Chemist's Guide to Density Functional Theory*, Wiley-VCH Verlag GmbH, Germany
- [61] **Gavnholt J.,**(2009). The Structure of Individual Nanoparticles and Hot Electron Assisted Chemistry at Surfaces, Ph.D. Thesis, Technical University of Denmark, KongensLyngby, Denmark
- [62] **Hammer B., Hansen L. B., Nørskov J. K.,**(1999). Improved Adsorption Energetics Within Density-Functional Theory Using Revised Perdew-Burke-Ernzerhof Functional, *Physical Review B*, **59**, 7413–21
- [63] **Vanderbilt D.,**(1990). Soft Self-Consistent Pseudopotentials In A Generalized Eigen-Value Formalism, *Physical Review B*, **41**, 7892-5
- [64] **Shannon D. F.,** (1970). Conditioning of Quasi-Newton Methods for Function Minimization, *Mathematical Computation*, **24**, 647-56

- [65] **Bahn S. and Jacobsen K.**,(2002). An Object-Oriented Scripting Interface to A Legacy Electronic Structure Code, *Computing in Science & Engineering*, 4, 56-66
- [66] **Kovtyukhova N. I., Mallouk T. E., Pan L., Dickey E. C.**,(2003). Individual Single-Walled Nanotubes and Hydrogels Made by Oxidative Exfoliation of Carbon Nanotube Ropes, *Journals American Chemical Society*, **125**, 9761-9
- [67] **Lu A. J. and Pan B. C.**,(2004). Nature of Single Vacancy in Achiral Carbon Nanotubes, *Physical Review Letter*, **92**(10), 105504.
- [68] **Ye Y., Ahn C. C., Witham C., Fultz B., Liu J., Rinzler A. G., Colbert D., Smith K. A., Smalley R. E.**,(1999). Hydrogen adsorption and cohesive energy of single-walled carbon nanotubes, *Applied Physics Letters*, **74**(16), 2307
- [69] **Senyer, A.** to be published. M.Sc. Thesis, Energy Institute, Istanbul Technical University, TURKEY
- [70] **Durgun E., Dag S., Bagci V. M. K., Gülseren O., Yildirim T., Ciraci S.**,(2003). Systematic Study of Adsorption of Single Atoms on A Carbon Nanotube, *Physical Review B*, **67**, 201401.
- [71] **Sun Q., Wang Q., Jena P., Kawazoe Y.**,(2005). Clustering of Ti on a C60 Surface and Its Effect on Hydrogen Storage, *Journal of American Chemical Society*, **127**, 14582-3
- [72] **Yang S. H., Shin W. H., Kang J. K.**,(2006). Ni adsorption on Stone-Wales defect sites in single-wall carbon nanotubes, *The Journal of Chemical Physics*, **125**, 084705
- [73] **Lim S. C., Jang J. H., Bae D. J., Han G. H., Lee S.**,(2009). Contact Resistance Between Metal and Carbon Nanotube Interconnects: Effect of Work Function and Wettability, *Applied Physics Letters*, **95**, 264103
- [74] **Yang C. K., Zhao J. J., Lu J. P.**,(2002). Binding energies and electronic structures of adsorbed titanium chains on carbon nanotubes, *Physical Review B*, **66**, 041403
- [75] **Wu X., Zeng X. C.**, (2006). Adsorption of transition-metal atoms on boron nitride nanotube: A density functional study, *The Journal of Chemical Physics*, **125**, 044711.
- [76] **Lee H., Ihm J., Cohen M. L., Louie S. G.**,(2009). Calcium-Decorated Carbon Nanotubes For High-Capacity Hydrogen Storage: First-Principles Calculations, *Physical Review B*, **80**, 115412

CURRICULUM VITAE



Candidate's full name: Süha Erhan Ünal

Place and date of birth: Istanbul, 1986

Universities and

Colleges attended:

B.Sc. Chemical Engineering,

Istanbul Technical University, 2004-2009

M.Sc.(ERASMUS)Galilée Institute,

Université Paris 13, 2010-2011